On the origin of the changes in color of Ag/Al2O3 catalysts during storage

Tesnim Chaieb, Dalil Brouri, Sandra Casale, Jean-Marc Krafft, Tiago da Silva, Cyril Thomas, Laurent Delannoy, Catherine Louis

On the origin of the changes in color of Ag/Al$_2$O$_3$ catalysts during storage

Tesnim Chaieb, Dalil Brouri, Sandra Casale, Jean-Marc Krafft, Tiago da Silva, Cyril Thomas, Laurent Delannoy and Catherine Louis*

Sorbonne Université, CNRS, Laboratoire de Réactivité de Surface, LRS, F-75005 Paris, France

Running title: Ageing of Ag/Al$_2$O$_3$ catalysts

* To whom correspondence should be addressed:
Dr. Catherine Louis
Sorbonne Université, UMR CNRS 7197, Laboratoire de Réactivité de Surface, 4 Place Jussieu, Case 178, F-75252, Paris, France
E-mail: catherine.louis@upmc.fr
Tel: + 33 1 44 27 30 50
Fax: + 33 1 44 27 60 33

1

Abstract

Despite the large number of catalytic studies involving Ag/Al_2O_3 catalysts, especially in deNO$_x$ reactions, the phenomenon of ageing observed during catalysts storage after preparation by impregnation followed by a calcination treatment, has not been reported earlier and rises questions. The present paper highlights firstly the colors of the calcined Ag/Al_2O_3 catalysts (white to yellowish) and the associated UV-visible spectra as a function of the Ag loading (0.5 to 4 wt% Ag), and secondly the gradual changes of color to grey/black and the associated UV-visible spectra when the samples are stored in ambient air or in vacuum in a desiccator in dark. These changes were found to be reversible when the samples are re-calcined.

The physico-chemical changes in the silver species during ageing were explained thanks to a comprehensive characterization study of the Ag/Al_2O_3 catalysts after calcination and after ageing. Several techniques such as UV-Visible spectroscopy, XRD, electron microscopy, XAS and photoluminescence were used. After calcination, in addition to highly dispersed Ag^+ species on alumina, the presence of Ag_n clusters of size smaller than 1 nm was found to be responsible for the yellowish color of the Ag/Al_2O_3 catalysts with Ag loadings higher than 2 wt% Ag and for the associated plasmon band at 350 nm. The ageing process was explained based on characterizations, coupled to a close examination of the literature data on the mechanisms of reduction of Ag^+ species, and on physico-chemical phenomena that can influence the color of various silver-containing materials, such as Ag^0 particle size, aggregation/redispersion and surface alteration. Consequently, the ageing process of the calcined Ag/Al_2O_3 catalysts, associated to sample darkening and to Ag plasmon band shift and broadening in the entire visible range, was proposed to result from the modification of the nature of the supported Ag phase: the reduction of Ag^+ species (by auto-reduction and/or photo-reduction), followed by the growth of Ag^0 particles, It is proposed that the Ag_n clusters may act as nucleation sites for the formation of larger Ag^0 particles and that the formation of aggregates is favored by an easy migration of Ag on alumina.

Key Words: Ag/Al_2O_3, ageing, color, UV-visible, XRD, electron microscopy, photoluminescence, XAS

1. Introduction

Silver-based catalysts, such as Ag/Al_2O_3, have been broadly studied in reactions such as selective reduction of nitrogen oxides by hydrocarbons [1-14], ethylene epoxidation [15, 16] and reactions of green organic synthesis [17]. The most used method to prepare and activate this type of catalyst is very simple; it consists in impregnating the alumina support with an aqueous solution of silver nitrate, followed by a drying step and a calcination treatment in air at around 600 °C. High temperature calcination leads to the formation of highly dispersed silver species on alumina as isolated $Ag^{\delta+}$ or Ag^+ species and small clusters of a few atoms, according to various studies involving techniques of characterization, such as UV-Visible spectroscopy [4-8], X-ray absorption spectroscopy [11, 18] and NO_x-temperature-programmed desorption [3, 19].

Our group also selected this preparation method to study Ag/Al_2O_3 catalysts in the reaction of NO_x reduction by propene [3, 19]. Along these studies, series of samples were prepared with different silver loadings (from 0.5 to 4 wt %), and two phenomena were observed: (i) after calcination at 600 °C, the color of the samples varied from white to yellowish as the Ag loading increased; (ii) during storage of the calcined samples, their color evolved and gradually turned grey or black. Color change was faster for the more highly loaded samples and when exposed to ambient air and light (a few days) rather than when stored in air and dark (a few weeks) or under vacuum and in dark (several months). Color changes were found to be reversible after the samples were re-calcined.

It was very intriguing for us not to find report of these phenomena in the catalysis literature. This is why we decided to investigate the reasons for these color changes, thanks to several characterization techniques (UV-Visible spectroscopy, XRD, electron microscopy, XAS and photoluminescence) and a close examination of the literature data, most often found in other fields than catalysis. The main question for color darkening during storage of the calcined samples is whether these changes arise from the aggregation of Ag^+ species and the formation of Ag_2O particles or from Ag^+ reduction and the formation of Ag^0 particles. In both cases, dark samples are expected since Ag_2O is brown black and a precipitate of Ag^0 particles from a $AgNO_3$ solution is black. For this reason, the paper starts with a review on the possible reasons found in the literature for color changes in Ag-containing samples, then the Ag/Al_2O_3 samples are characterized after calcination and after ageing. The series of Ag/Al_2O_3 samples investigated in the present study corresponds to those studied earlier [3, 19].

2. Review on color changes in Ag-containing materials

In the literature, changes in sample color and evolution of the associated absorption band in UV-Visible are almost always reported in the case of samples initially containing metallic silver particles. Generally speaking, the evolution of the optical properties of metal nanoparticles (surface plasmon resonance (SPR) band) [20] can result from the evolution of several of their features: proportion of metallic species, density, size and size distribution of metal particles, interactions/distance between particles (for instance whether they aggregate or redisperse), and/or their environment that modifies the dielectric constant around the particles (for instance, the nature of the support or a shell covering the metal particles).

2.1. Changes of size of Ag^0 particles and/or in their distances

An example illustrating the influence of particle size on the optical properties concerns Ag^0 nanoparticles introduced in wool to color it. Various colors were obtained depending on the particle size, i.e., depending on the sodium citrate concentration used to reduce the silver ions in aqueous solution [21]. The wool became (i) yellow/orange when it contained 10 to 15 nm Ag particles with a SPR band at 430 nm, (ii) red/brown with 20 nm Ag particles, isolated and aggregated, as well as larger particles, leading to a SPR band at 480 nm, (iii) brown/black when the wool contained 10 to 100 nm Ag particles, which led to an absorption band in the whole visible region.

Another example illustrating the effect of aggregation/redispersion is related to a thermo-chromic effect observed in materials consisting of Ag^0 particles embedded in a polystyrene matrix [22]. The color changed as a result of the reversible aggregation of 3 nm Ag particles caped with thiols. At RT, the sample was brown, and the Ag particles were aggregated because of the inter-digitation of the linear alkyl-thiolate chains stabilizing the Ag nanoparticles. In contrast, when the sample was heated at 160 °C, it turned yellow because of an increase in the inter-particle distance. The yellow sample showed a plasmon band at 430 nm, while the plasmon band of the brown sample showed an enlargement up to 750 nm due to the presence of a second component at 560 nm, resulting from the aggregation of Ag particles.

Ritzer et al. [23] showed that the phenomenon of aggregation was reversible. They reported that a sample consisting of silica sol-gel glasses doped with Ag^0 particles reversibly changed of color several times, from yellowish to darker and *vice-versa*, through alternate treatments in air at 600 °C and at 60 °C for 24 h or at RT for several weeks. Alternate darkening-bleaching was explained by a phenomenon of reversible aggregation-disaggregation of silver particles (70-80

nm at 60 °C at RT and 30-60 nm after treatment at 600 °C), leading to an increase-disappearance of a broad SPR absorption centered at 420 nm. The authors also reported that sample darkening occurred in ambient air whether the particles were exposed to natural light or not.

2.2. Evolution of the Ag^0 particles in air

It is well-known that silver artifacts tarnish and blacken in ambient air. This does not result from surface oxidation by O_2, but from surface sulfidation by sulfur compounds present in ambient air in very low concentrations, such as H_2S, OCS and SO_2 [24-26]. Surface alteration was also found to take place on silver nanoparticles, which affects the SPR response, since the environment of the particles is modified. Such surface reactions were observed for Ag nanoparticles of different sizes (a few nm to hundreds of nm), different shapes (spheres, rods, disks), supported on various substrates (quartz slides, ITO-coated glass slides, alumina film …) and synthesized by different chemical or physical techniques [27-32]. This results in a SPR red-shift or blue-shift of tenths to hundreds of nm, depending on the size and shape of the Ag particles and the duration of the exposure to air, as a consequence of two antagonist phenomena: (i) the formation of a sulfide shell around the Ag particles, which induces a plasmon red-shift; (ii) the shrinking of the Ag^0 particle core when the sulfide shell thickens or when the particles disrupt, which induces a plasmon blue-shift. The predominance of one or the other factor depends on the initial size of the Ag particles. For instance, for Ag^0 nanoparticles (35 nm) deposited by atomic sputtering on an Al_2O_3 layer [31], the SPR band intensity decreased by a factor of 14 after 12 months in ambient air, and the maximum of the SPR band shifted from 465 to 435 nm. The detection of S by XPS indicated the formation of a sulfide.

The stability of the Ag^0 nanoparticles also depends on the nature of the substrate, and surface alteration can result from oxidation and not only from sulfidation. Pelaez et al. [33] compared the behavior in air of Ag^0 particles of small sizes (1.6, 2.1 and 4.3 nm) deposited on glass and on Al_2O_3 film by pulsed laser deposition. In ambient air, the SPR band blue-shifted from 520 to 470 nm with Al_2O_3 film and from 500 to 440 nm with glass. The shifts were accompanied by a decrease in the SPR band intensity, but more rapidly on Al_2O_3 than on glass (70 against 20% of intensity decrease after 25 months in air) and by color changes as the samples, initially blue gray, turned yellowish in air. The Ag particles also became larger than 10 nm in both samples, and elongated 100 nm-long particles appeared on Al_2O_3. XPS and Auger analyses revealed the formation of a thin shell of sulfided Ag (1% S) around the Ag particles supported on glass and of a deeper layer of oxidized Ag (Ag-O) on the Ag particles on Al_2O_3.

These differences were attributed to different metal-support interactions according to the nature of the support. The blue-shift resulting from the shell growth at the expense of the size of the metal core, compensated the small red-shift induced by the higher refractive index value of the shell than in air.

The stability of the Ag^0 nanoparticles was also reported to depend on the nature of the surrounding atmosphere, ambient air or pure O_2. For instance, for Ag^0 nanoparticles supported on silica and alumina, the SPR band red-shifts were smaller and the decrease of intensity weaker when the samples were exposed to pure O_2 than to air. The difference was attributed to the presence of water in air.

Moreover, recent studies have shown that much more complex compositions than silver sulfide (Ag_2S) could form on metal silver plates exposed to ambient air at RT, depending on the local conditions, outdoor sites, such as marine, volcanic, rural, alpine sites and suburban sites, or indoor sites, such as showcases of museums: silver chloride (AgCl), silver oxide (AgO), silver sulfite (Ag_2SO_3), silver sulfate (Ag_2SO_4) and silver carbonate (Ag_2CO_3) were detected by XPS or voltammetry in larger proportion than silver sulfide and in proportion dependent on the type of ambient air [34-36]. The formation of a basic carbonate ($AgOHAg_2CO_3$) was also detected by *in situ* coupled IRRAS/QCM technique on polycrystalline silver prepared by physical vapor deposition on quartz and exposed to synthetic air containing CO_2 (125-1000 ppm) and water (50 and 90% of relative humidity), under or without UV irradiation [37] Additional *ex situ* TOF-SIMS measurements revealed the presence of three products on the Ag surface, Ag_2CO_3, Ag_2O and AgOH, the 3-dimensional distribution of which was dependent on the experimental conditions. It turns out that the presence of water in air is of prime importance. Several other papers also reported that both sulfidation and oxidation require humidity to take place [38-41].

3. Experimental

3.1. Catalyst preparation

The γ-Al_2O_3 support (Procatalyse, 180 m^2/g) was ground and sieved, and the fraction between 200 and 315 μm was used to prepare the Ag samples. As mentioned in the introduction section, Ag deposition was performed by incipient wetness impregnation of the Al_2O_3 support with aqueous solutions of $AgNO_3$ (Aldrich, purity >99 %) (0.7 cm^3/g_{Al2O3}) with different concentrations to achieve silver loadings from 0.5 to 4 wt%. After impregnation, the samples were aged for 4 h in ambient air then dried overnight at 100 °C in air. Finally, they were calcined

at 600 °C for 4 h in a muffle furnace after a 3 °C/min heating ramp. The samples were denoted Ag(x)/Al$_2$O$_3$, where x represents the silver loading expressed in wt%. Just after impregnation and calcination, the samples were noted "calcined samples". After aging in conditions described later, they were re-calcined under the same conditions as the first calcination treatment.

3.2. Characterization techniques

The silver loadings were determined by inductively-coupled plasma atomic emission spectroscopy (ICP-AES, Crealins – Solaize).

The diffuse reflectance ultraviolet–visible spectra of the Ag/Al$_2$O$_3$ samples were collected on a Varian Cary 5000 spectrophotometer at RT and in ambient air, from 200 to 600 nm, using the calcined Al$_2$O$_3$ support as the reference background. Measurements were carried out on samples, calcined, aged for different durations, after re-calcination at 600 °C and also after reduction at 550 °C (3 °C min^{-1}, under 20 % H$_2$ in He (100 mL$_{NTP}$ min^{-1}), 2 h at 550 °C) or after NO$_x$ Temperature-Programmed Desorption experiments (NO$_x$-TPD) in the same conditions as those reported in [3, 42]. Briefly, after NO$_x$ adsorption under a gas mixture containing 385 ppm NO and 8% O$_2$ in He (230 mL$_{NTP}$ min^{-1}), the samples were heated from RT to 550 °C (3 °C min^{-1}) under 8% O$_2$ in He.

Transmission Electron Microscopy (TEM) was performed at the Plateform of Electron Microscopy of the Institut des Matériaux de Paris Centre of Sorbonne Université. Bright field TEM images were obtained with a JEOL 2010+ microscope operating at 200 kV and equipped with an Orius CCD camera (Gatan), while HRTEM and energy dispersive X-ray spectroscopy (X-EDS) characterizations were performed using a JEOL 2100+ microscope equipped with SDD detector (Oxford X-max) for X-EDS and an Orius CCD camera (Gatan). In addition, aberration-corrected scanning transmission electron microscopy (STEM) imaging was also carried out on the Ag(2.6)/Al$_2$O$_3$ sample at the University Paris Diderot, using a JEOL ARM 200F microscope, operating at 200 kV and fitted with a high angle annular dark field (HAADF) detector. Sample preparation for TEM observations consisted of the direct deposition of the dry powder after grinding, onto amorphous carbon-coated copper TEM grids. Indeed, powder dispersion in ethanol is known to induce severe sintering of the Ag particles [43].

XRD measurements were carried out from 10 to 80° by step of 0.01° using a theta-theta D8 Advance (Bruker) powder diffractometer with Cu-Kα radiation source (0.154 nm) operating at 30 kV and 30 mA, and equipped with a 1D LynxEye detector set to a 3° opening.

Photoluminescence spectra were recorded using a spectrofluorophotometer Horiba Fluorolog 3 equipped with a 450 W Xe lamp as an excitation source, and a UV filter to cut the excitation light below 295 nm. The excitation and emission bandwith were set to 5 and 2 nm, respectively, and the acquisition time was 3s/nm. The emission photoluminescence spectra were obtained for the excitation wavelength at 280 nm. The spectra were recorded at around 10 K using liquid helium after sample outgassing (10^{-6} - 10^{-7} Torr) overnight at RT under dynamic vacuum.

XAS measurements were conducted at the Ag K edge (25514 eV) at the ROCK beamline of the SOLEIL synchrotron using a monochromator equipped with a Si(220) channel-cut crystal. Ag/Al_2O_3 samples as well as reference samples ($AgNO_3$ and Ag_2O) were diluted with boron nitride and pressed as pellets. They were analyzed at room temperature in the transmission mode, and with an Ag metal foil used as standard for energy calibration at 25514 eV. Spectra extraction and analyses were carried out with the IFEFFIT library provided by the Demeter package with softwares Athena and Artemis [44]. EXAFS spectra were extracted in Athena with $R_{bkg} = 1.4$ cut-off and k weight = 3. Fourier-transformed (FT) EXAFS spectra were obtained with a Hanning window in k^3 (k = 3.3 - 9.0) with a dk = 1.0. EXAFS fitting was done with Artemis using the amplitude reduction factor (S^2_0) of 0.821, as determined by EXAFS fitting of the Ag metal foil. The scattering paths for Ag-O and Ag-Ag were obtained by simulation with the ATOMS algorithm with input files of the crystal structures of Ag_2O (Ag-O) and Ag metal (Ag-Ag). EXAFS parameters were calculated by FT-k^3 least-square fitting. The goodness of fit was determined by observing the reduced χ^2 and R^2 statistical parameters.

4. Results and Discussion

4.1. Basic characterizations
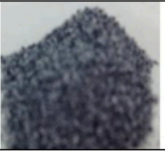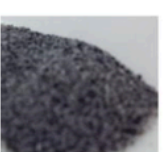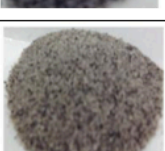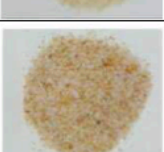
4.1.1 Color changes

As mentioned in the introduction section, the color of the calcined Ag/Al_2O_3 samples depends on the silver loading and the duration and conditions of storage. The calcined Ag(0.5 to 1.8)/Al_2O_3 samples were white while the Ag(2.2 to 4.1)/Al_2O_3 ones were slightly yellowish (Column A in **Table 1**). Column B in **Table 1** shows examples of color evolution after the samples were kept in vials in air and in dark for 12 months: black grains appeared in the samples, and the whole color darkened. Color evolution was faster when the samples were stored in vials exposed to light and air, and much slower when they were stored under vacuum and in dark. It also depended on the Ag loading, the higher the Ag loading, the faster the color

evolution. For instance, the Ag(3)/Al$_2$O$_3$ sample, yellowish after calcination, turned black after around one week in air and light or after a month in air and dark, but was still yellow after 5 days in vacuum and dark, and did not turn completely black after extra two years. The color of the aged Ag/Al$_2$O$_3$ samples almost changed back to their original color (Column C in **Table 1**) when they were subjected to a re-calcination treatment. One can note that after a reduction treatment at 550 °C under H$_2$ (20% in He) for 2 h, the reduced samples were uniformly brown.

To understand the origin of the color changes and identify the oxidation states of silver, the samples were first characterized by UV-visible spectroscopy, electron microscopy and X-ray diffraction, then by photoluminescence and XAS. TPR-TPO and XPS were found to be useless for this study (**SupInf1**).

Table 1: Color of the Ag(x)/Al$_2$O$_3$ samples, (A) freshly calcined at 600 °C; (B) aged 12 months in air and dark; (C) re-calcined at 600 °C

Sample	calcined (A)	aged 12 months in air (B)	re-calcined (C)
Ag(0.5)/Al$_2$O$_3$			
Ag(0.9)/Al$_2$O$_3$			
Ag(1.8)/Al$_2$O$_3$			
Ag(2.2)/Al$_2$O$_3$			
Ag(2.6)/Al$_2$O$_3$			
Ag(3.5)/Al$_2$O$_3$			
Ag(4.1)/Al$_2$O$_3$			

4.1.2. UV-visible spectroscopy

Figure 1A shows the UV-visible spectra of a series of calcined samples (white to yellowish according to **Table 1**). All of the spectra look roughly similar, and exhibit three bands at 210, 240 and 350 nm, and the overall intensity of the spectrum increases with the Ag loading. The UV-visible spectra (**Figure 1B)** of the 12 month-aged Ag/Al_2O_3 catalysts (grey/black, column B in **Table 1**) still show the two bands at 210 and 240 nm, but they are less resolved and relatively less intense than in **Figure 1A**. They also show a band at 300 nm and a broad and flat absorption band between 320-350 nm and 600 nm due to sample darkening. An exception is the sample with the lowest loading, $Ag(0.5)/Al_2O_3$, whose color remained lighter, and the spectrum showed instead a low intense band with a maximum at 420 nm. The UV-visible spectra in **Figure 1C** of the Ag/Al_2O_3 samples aged for 12 months then re-calcined at 600 °C again show the three bands at 210, 240 and 350 nm and an overall absorption slightly higher than for the freshly calcined samples (**Figure 1A**), which is consistent with the fact that the colors of both series of samples are almost the same (**Table 1**), and which indicates that the process of aging is reversible.

Figure 2 compares the UV-visible spectra of sample $Ag(2.6)/Al_2O_3$, calcined (yellowish) (**spectrum a**) then recorded after different ageing times and thermal treatments. The spectra of the sample aged for 12 and 24 months (both grey samples) look very similar (**spectra b and c**). As mentioned above, the spectra of the calcined (**spectrum a**) and of the 12 month-aged sample re-calcined at 600 °C (**spectrum d**) look similar in shape. Interestingly, when the aged sample was treated under the conditions of NO_x-TPD (see **Section 3.2**), it turned perfectly white, and did not show any band at 350 nm, and the band at 240 nm was clearly more intense (**spectrum e**). For comparison, the sample reduced at 550 °C under H_2, which had a brown color as mentioned above, showed a broad band at around 420 nm (**spectrum f**).
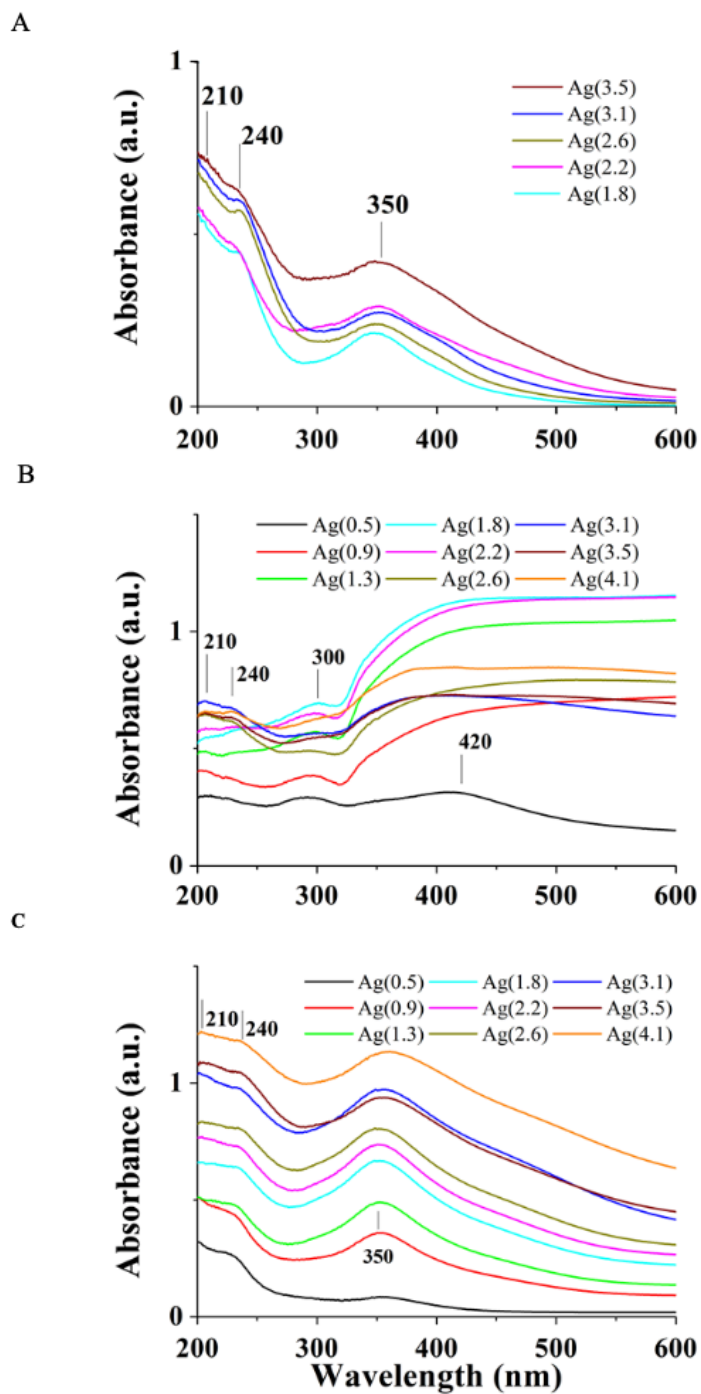
Figure 1: UV-visible spectra of Ag(x)/Al$_2$O$_3$ samples (**A**) calcined at 600 °C; (**B**) aged for 12 months in air; (**C**) re-calcined at 600 °C.
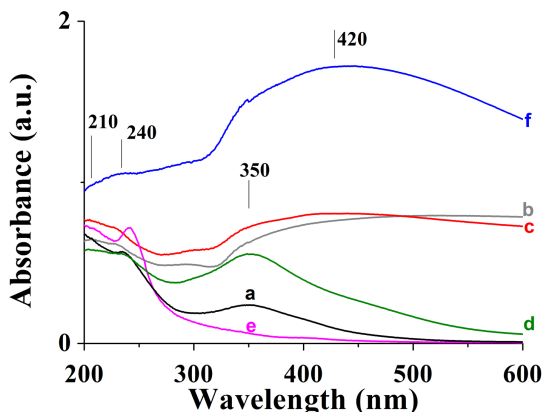
Figure 2: UV-visible spectra of Ag(2.6)/Al$_2$O$_3$ (a) calcined at 600 °C, (b) 12 month-aged, (c) 24 month-aged, (d) 12 month-aged and re-calcined at 600 °C, (e) calcined then submitted to NO$_x$-TPD, (f) 12 month-aged in air and reduced at 550 °C under H$_2$ (20% in He).

4.1.3. X-ray diffraction and Electron microscopy

Calcined, reduced and aged Ag(2.6)/Al$_2$O$_3$ samples were examined by XRD (**Figure 3**). After calcination, reduction and ageing (**Figure 3b,c,d**), no other peak than those of alumina (**Figure 3a**) could be observed. For the calcined sample, this is not surprising since Ag was expected to be highly dispersed on alumina [11, 18]. In the case of the reduced sample, the absence of Ag^0 peaks could mean that the Ag^0 particles are very small. However, the three most intense peaks of Ag^0 expected at 38.1, 44.3 and 64.4° (JCPDS 65-2871) and the main peak of Ag$_2$O expected at 32.8° (JCPDS 41-1104, I =100), could be present but masked by the intense peaks of alumina in the diffractograms of the reduced and the calcined samples, respectively. Aged samples with higher loadings (3.5 and 4.1%) showed additional thin peaks (**Figure 3e,f**) forming two sets of three peaks, set 1 at 32.8, 33.9 (higher) and 34.4° (shoulder), and set 2 of lower intensity at smaller angles, 18.8, 19.6 (higher) and 20.8° as well as very small peaks at 49.0 and 51.6°. These peaks do not match with the diffraction patterns of Ag^0, and only the peak at 32.8° is at a position close to the main one of Ag$_2$O (**Table 2**). The peak positions were then compared to the most intense ones of several Ag compounds (**Table 2**). Part of the peaks of Ag$_2$S could match with those of the more intense set of three peaks (set 2). The other ones of Ag$_2$S could be hidden by the broad and intense peaks of alumina. However, the rather intense peak of Ag$_2$S at 28.9° does not match at all, and no peak correspond to those of set 1. Moreover, no sulfur could be detected in our samples by XPS (see **SupInf1**) and X-EDS (see **SupInf4**), so the formation of Ag$_2$S during ageing can be discarded. Some peaks of AgO could match with two peaks of set 2 but not with the strongest one, and anyway, AgO is known to be unstable (see **Equation 1** in **Section 4.4**). The best match was obtained with silver carbonates. Ag$_2$CO$_3$

exists under three structures: monoclinic, hexagonal α-phase and hexagonal β-phase. **Table 2** shows that the two sets of three peaks could correspond to a mixture of monoclinic and hexagonal α-Ag₂CO₃, but the presence of hexagonal β-Ag₂CO₃ peaks cannot be formally excluded. In addition, the peaks of these Ag₂CO₃ structures match the tiny peaks observed at around 50-55° (**Figure 3**). We also checked that none of the peaks of the two sets match with the most intense ones of other silver compounds, such as AgCl, Ag₂SO₄, Ag₂SO₃ and silver aluminate (see **SupInf2**).
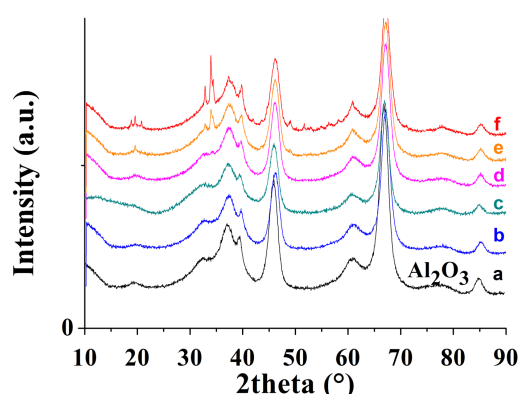
Figure 3: XRD patterns of (a) Al₂O₃, (b) Ag(2.6)/Al₂O₃ calcined at 600 °C, (c) Ag(2.6)/Al₂O₃ 12 month-aged then reduced at 550 °C in H₂, (d) Ag(2.6)/Al₂O₃ aged 24 months, (e) Ag(3.5)/Al₂O₃ 24 month-aged, (f) Ag(4.1)/Al₂O₃ 24 month-aged.

Table 2: Selection of silver or aluminum compounds whose XRD peaks (extracted from the JCPDS files) match with some of the new peaks appearing during ageing of Ag(4.1)/Al₂O₃ sample. I: peak intensity

	aged Ag/Al₂O₃	γ-Al₂O₃ 10-0425 (blank)	Ag⁰ 65-2871 (indexed) I≥46	Ag₂S 14-0072 (high) I≥45	Ag₂O 41-1104 (high) I≥28	AgO 84-1547 (high) I≥35	Monoclinic Ag₂CO₃ 26-0339 (high) I≥30	Hexagonal α-Ag₂CO₃ 31-1237 (high)	Hexagonal β-Ag₂CO₃ 31-1236 (high)
set 1	18.8						18.5 (020) I=35		
	19.6 (highest)	19.5° (111) I=40						19.5 (110) I=50	19.3 (110) I=25
	20.8						20.5° (110) I=30		
set 2	32.8			28.9° (111) I=60 * 31.5° (-112) I=70	32.8° (111) I=100	32.0° (200) I=48 32.3° (-111) I=100	32.5° (-101) I=60		
	33.9 (highest)			33.6° (120) I=45			33.6° (-130) I=100	33.3 (111) I=100	33.8 (300) I=100
	34.4 (shoulder)			34.4° (-121) I=100 34.7° (022) I=70		34.2° (002) I=35		34.1 (300) I=60	
Al₂O₃	37.2	37.6° (311) I=80	38.1° (111) I=100	36.6° (112) I=70 36.8° (121) I=80 37.1° (013) I=60 37.7° (-103) I=75	38.1° (200) I=28	37.1° (111) I=87			
	39.4	39.5° (222) I=50				36.4° (-202) I=37	39.6° (031) I=35		
	46.0	45.8° (400) I=100	44.3° (200) I=46						
	60.5	60.9° (511) I=30							
	67.1	67.0° (440) I=100							
	84.8	85.0° (444) I=20							

* the peak of Ag₂S that does not match the experimental results

The Ag(2.6)/Al$_2$O$_3$ samples, freshly calcined, aged, reduced and re-calcined after aging, were also examined by electron microscopy. No particles other than those of alumina could be observed in the calcined and in the re-calcined samples. Small Ag particles were observed in the reduced one (**Figure 4A)** with an average size of 3.7 nm (size distribution in **SupInf3**). In the case of the aged sample, silver particles could be observed by TEM, forming both silver aggregates of 30-50 nm (**Figure 4Ba**) as confirmed by X-EDS measurements (see **SupInf4**), and small particles (**Figure 4Bb)** of 2.3 nm (size distribution in **SupInf3**). Again, the absence of Ag particles on alumina in the calcined sample is not surprising since Ag is expected to be highly dispersed on such a sample. Re-calcination confirmed that the ageing process was reversible.

HRTEM was performed on silver nanoparticles (NPs) and aggregates in the aged sample to evaluate the inter-reticular distances from the lattice fringe spacings and to deduce the nature of the Ag species. It was difficult to find crystal planes on nanoparticles and aggregates of Ag(2.6)/Al$_2$O$_3$: nanoparticles were very small and aggregates were polycrystalline with various thicknesses and orientations. However, a significant number of measurements could be done on aggregates in the aged Ag(4.1)/Al$_2$O$_3$ sample and on nanoparticles of the aged Ag(3.0)/Al$_2$O$_3$ sample (**Table in SupInf5**). The most frequent lattice distance values measured were 2.0-2.1 and 2.3-2.4 Å, both for nanoparticles and aggregates. They were compared to the lattice distances of several Ag compounds, Ag^0, Ag$_2$O, Ag$_2$S, Ag$_2$CO$_3$, Ag$_2$SO$_4$, Ag$_2$SO$_3$ and AgCl. The two sets of values match very well with the lattice distances of the two most dense planes of Ag^0, (200) and (111), with d_{200} =2.04 Å and d_{111} =2.35 Å. The discussion on the assignment of the other distances measured is detailed in the supplementary material (**SupInf5**). Hence, data analysis of the HRTEM images indicates that the aggregates and nanoparticles in the aged samples are mainly Ag^0.

These first characterizations lead to the conclusion that the ageing process induces the formation and growth of Ag^0 aggregates and nanoparticles, the sizes of which are larger than those formed during thermal reduction, but that silver carbonates are also present in the highly loaded samples. Before going further in the study of the ageing process, it is important to have a clear view of the state of the Ag/Al$_2$O$_3$ samples after calcination.
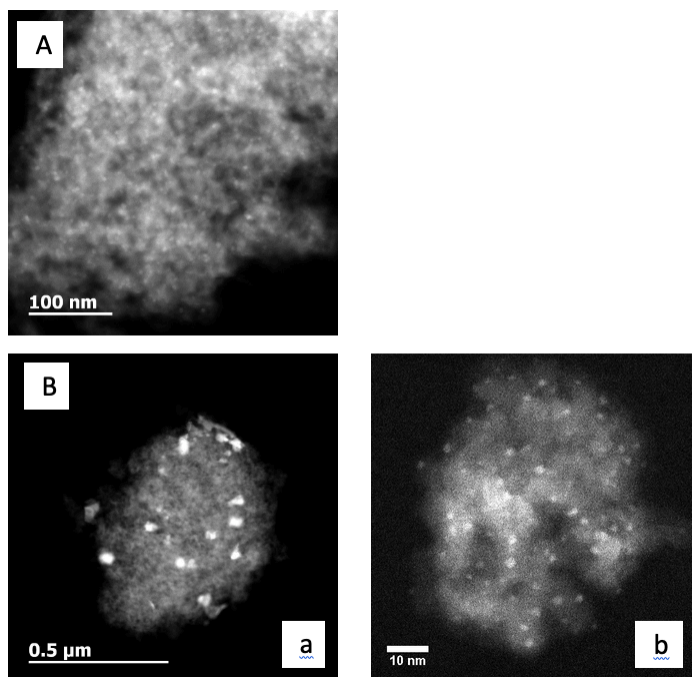
Figure 4: HAADF-STEM images (dark field) (A) of 12 month-aged Ag(2.6)/Al$_2$O$_3$ then reduced at 550 °C (B) 12 month-aged Ag(2.6)/Al$_2$O$_3$: (a) large aggregates, (b) small particles

4.2. Discussion on the nature of the Ag species present in the Ag/Al$_2$O$_3$ catalysts

4.2.1. Ag species in the calcined Ag/Al$_2$O$_3$ samples

There is a general agreement in the literature for assigning the two weak absorption bands at around 210 and 230-240 nm in the UV-visible spectra of the samples calcined at 600 °C (**Figure 1A**) to isolated Ag$^+$ ions [4, 6-8, 45]. This attribution is based on the seminal paper of Texter et al. [46] who reported the UV-visible spectra of aqueous solutions of several kinds of silver salts. Other papers reporting the same type of spectra for Ag/Al$_2$O$_3$ samples as those shown in **Figure 1A** are summarized in **Table 3.**

The broad band centered at 350 nm absorbing in the violet range is responsible for the yellowish color of the samples, and for the stronger coloration of the highly loaded samples. This band is however also present in the Ag(1.8)/Al$_2$O$_3$ sample that appears white in **Figure 1A**. The attribution of this band at 350 nm is discussed below. Let us remind first that the yellowish sample Ag(2.6)/Al$_2$O$_3$ turned white after NO$_x$-TPD up to 550 °C, and that the UV-visible spectrum did not show the band at 350 nm any longer, but an increase in intensity of the band around 240 nm (**Figure 2a and e**). UV-visible spectra similar to that shown in **Figure 2e** were reported by Richter et al. [7] for 1 and 5% Ag/Al$_2$O$_3$ after *in situ* calcination at 500 °C and by Bethke et al. [4] for 2 and 6% Ag/Al$_2$O$_3$ after calcination at 700 °C (**Table 3**). Bethke et al.

mentioned in their paper that the samples were white, and that no Ag peak was detected by XRD. The general conclusion of these two papers was that the calcined Ag/Al$_2$O$_3$ catalysts contained isolated Ag$^+$ ions (200-230 nm), but also small Ag$_2$O particles whose presence was attested by TPR [4, 47]; note that Ag$_2$O was claimed as UV-visible silent [48]. To our knowledge, only Aneggi et al. [49] could detect Ag$_2$O (10-20 nm) and Ag^0 particles by HRTEM in samples of silver supported on Al$_2$O$_3$ samples, but their TEM grids were prepared from a sonicated suspension of the samples in ethanol and, as mentioned in section Experimental, such a type of grid preparation induces severe enlargement of silver particles [43].

Table 3: UV-Visible absorption bands and assignments of various Ag/Al$_2$O$_3$ samples prepared by impregnation with AgNO$_3$ followed by calcination and by reduction

Sample	Calcination temperature (°C)	UV-Visible bands (nm)	Assignment	Reduction temperature (°C)	UV-Visible bands (nm)	assignment	ref
0.5 to 4.1% Ag/γAl$_2$O$_3$ (180 m^2/g)	600	~210 and ~230 350		550	420	Ag^0 NPs (brown)	This work
1 and 5% Ag/mesoporous- Al$_2$O$_3$ (400 m^2/g)	500 (*in situ*)	200-250	Ag$^+$	Up to 550 (*in situ*)	235-240 400	Atomic Ag^0 into Al$_2$O$_3$ defect sites Ag^0 clusters **	[7]
2 and 6% Ag/γ Al$_2$O$_3$ (200-250 m^2/g)	700	200-230	Ag$^+$	700	400	Ag^0 NPs (rust)	[4]
1.5% Ag/ Al$_2$O$_3$ (sol-gel) (170 m^2/g)	650	190 and 220 ~350	Ag$^+$ Ag$_n^{\delta+}$ clusters	Up to 600 (*in situ*)	420	Ag^0 NPs	[45]
10% Ag/γ Al$_2$O$_3$		240 270-290 and 370-390 315 420-460	Ag$^+$ Ag$_n^{\delta+}$ Ag film* Ag^0 NPs/aggregates				[48, 53]
1.2 and 10% Ag/γ Al$_2$O$_3$ (150 m^2/g)	630	210 and 230 290 and 350 >390	Ag$^+$ Ag$_n^{\delta+}$ clusters Ag^0 NPs	630	210 and 230 290 and 350 >390	Ag$^+$ Ag$_n^{m+}$ Ag^0 NPs	[6]
4% Ag/γ Al$_2$O$_3$ (185 m^2/g)	600	223 290 and 352	Ag$^+$ Ag$_n$ clusters	600	223 352	Ag$^+$ Ag$_n$ clusters	[52]
0.25 to 5% Ag/γ Al$_2$O$_3$ (150 m^2/g)	550	240 305 360 400 (≥3%Ag)	Ag$^+$ Ag$_n^{\delta+}$ clusters Ag$_n^0$ clusters Ag^0 NPs				[12]
2% Ag/ Al$_2$O$_3$ (sol-gel) 0.6 to 5% Ag/γ Al$_2$O$_3$ 5% Ag/γ Al$_2$O$_3$	800 500 500	220-230 220-230 220-230 and 280-350	Ag$^+$ Ag$^+$ Ag$^+$ and Ag$_n^0$ clusters				[8]
3.8% Ag/γ Al$_2$O$_3$ (200 m^2/g)	550	230 260 290 and 350	Ag$^+$ Ag$_n^{\delta+}$ Ag$_n^0$ clusters				[86]
1.4% Ag/γAl$_2$O$_3$ (220 m^2/g)				100, 200	233 420	Ag$^+$ Ag^0 NPs	[87]

* associated with the intrinsic photoeffect of Ag, i.e., the interband transition observed in bulk Ag (electron transition from the valence band to conduction band, the threshold of which is 4 eV, i.e. 310 nm) [20]
** the difference with Ag^0 NPs is not clear

The assignment of the band at 350 nm can now be discussed. Several attributions were proposed in the literature as shown in **Table 3**. The band was sometimes associated to another one at 280-290 nm and attributed to Ag$_n^0$ or Ag$_n^{\delta+}$ clusters, i.e., to ensembles of small number of Ag atoms (<10-20 atoms) carrying no charge or a δ+ charge: (i) Ag$_n^{\delta+}$ clusters for bands at at 260-268 nm with 2≤n≤4 [50], 290 and 350 nm [6], 305 nm [12], ~350 nm [45], 360 nm [12]; (ii) Ag$_n^0$ clusters for bands at 280-350 nm [8], 285 and 345 nm [51], at 290 and 352 nm [52],

16

360 nm [12].

If one carefully examines the origin of the band assignments in these papers, one can note that they arise from (i) a series of papers published in 1986-1996 by Davydov and coll. (mostly in Russian) on Ag supported on various oxides [48, 53], (ii) papers studying the formation of Ag_n clusters in solid Ar matrices at low temperature [54, 55] and in zeolites [56], and (iii) papers published in the 80-90[ths], which investigated the formation of Ag colloids in liquid phase from Ag^+ reduction by radiolysis under γ-irradiation [57-60]. Among them, the paper by Henglein and coll. [60] reported that Ag_2^+ gave absorption bands at 265 and 310 nm, Ag_4^{2+} gave a band at 280 nm, three other unidentified clusters gave bands at 330, 330 and 345 nm, Ag_8^+ gave bands at 290 and 325 nm, Ag_n^+ with n<10 a band at 360 nm, whereas Ag^0 NPs gave a band at 380 nm. All the interpretations concerning the band at ~350 nm converge to the conclusion that it is related to the presence of Ag_n clusters. Whether the Ag_n clusters are neutral (Ag_n^0) or slightly positively charged ($Ag_n^{\delta+}$) probably depends on the interaction between the Ag cluster and the support, i.e., on possible charge transfer. In addition, this band is the result of the phenomenon of surface plasmon resonance (SPR) of these small clusters. Indeed, for silver, and in contrast with gold, even tiny Ag particles [20] or clusters of less than 20 atoms, whether they are neutral [61] or ionic [62], generate surface plasmon resonance like much larger metallic Ag particles. Ag^0 nanoparticles smaller than 10 nm, such as silver colloids in water, are yellow, and exhibit a SPR absorption band at around 400 nm [63-65]. A yellow color has also been reported for Ag^0 particles interacting with a support [22, 65, 66]. Since no Ag particles are detected by XRD or TEM in our calcined samples, this means that they are smaller than 1 nm (i.e., containing less than 50 atoms). Accordingly, Pal and De [65] could not observe either any nanoparticles in a yellow Ag/porous silica film calcined in air at 450 °C. Hence, the band at 350 nm and the yellow color of our samples can result from the SPR of Ag_n clusters, neutral or slightly positively charged and containing a small number of Ag atoms. This assignment is also consistent with the fact that when the samples were submitted to a NO_x-TPD experiment, i.e., to NO and NO_2 which are more oxidizing gas than O_2, the band at 350 nm disappeared, while the band at 240 nm attributed to Ag^+ was more intense than after calcination (**Figure 2**) and the samples turned white because Ag was present only as isolated Ag^+ species.

The small band at 300 nm observed only in the UV-Visible spectra of the aged samples (**Figure 1B**), but which could have been hidden by the band at 350 nm in the calcined (**Figure 1A**) or in the re-calcined samples (**Figure 1C**), can be tentatively attributed to $Ag_n^{\delta+}$ clusters if one refers to a paper of Sadokhina et al. [12]. These authors assigned the presence of a band at

305 nm (not always clearly visible in a set of calcined Ag/Al_2O_3 samples with 0.25 to 5 % Ag) to $Ag_n^{\delta+}$ clusters of smaller size than the Ag_n^0 clusters associated to a band at 360 nm.

Hence, after calcination, the Ag species present on the alumina support are isolated Ag^+ ions, associated to the UV bands at 210-230 nm, and Ag_n clusters, associated to the SPR band at ~350 nm (these clusters are Ag_n^0 or $Ag_n^{\delta+}$, but for the sake of simplicity, they are called Ag_n clusters in the following).

The formation of silver aluminate during Ag/Al_2O_3 calcination was evoked in a few papers, but was not experimentally proven [7, 8, 45], except indirectly in the paper of Bogdanchikova et al. [6]. Using a phase refinement procedure, the authors were able to extract the XRD pattern of $AgAl_{11}O_{17}$ from that of alumina in a 10% $Ag/\gamma Al_2O_3$ sample calcined at 630 °C. However, silver aluminate usually forms under much more severe conditions, at 800 °C under 10% of H_2O in air for a 2% Ag/Al_2O_3 sample [67] or at 850 °C in air for a 22% Ag/Al_2O_3 sample [10]. Thus, we think that its presence can be discarded in our samples.

One can wonder why all silver did not remain in the oxidation state +1 (i.e., in oxidized state) during calcination and why Ag_n clusters formed. It is known that bulk Ag_2O decomposes into Ag^0 in air at around 200 °C [68], and also that supported Ag_2O nanoparticles or Ag^+ ions are more stable and decompose at higher temperatures. For instance, in a 5% Ag/Al_2O_3 sample, Ag^0 and Ag_2O were detected by XRD after calcination at 500 °C, and only Ag^0 after calcination at 850 °C [49]. Cai and coll. [69] reported that in 0.12 to 2.4% Ag/SiO_2 samples, no SPR band was observed in UV-Visible spectra after calcination in air at 500 °C, whereas a SPR at 420 nm was observed after calcination at 700 °C, but of much weaker intensity than in a sample reduced in H_2 at 500 °C. Their conclusion was that the smaller the Ag_2O particles, the higher the decomposition temperature in air into Ag^0. Coming back to the present Ag/Al_2O_3 samples, one can anticipate that all the Ag^+ species cannot atomically disperse during calcination [3, 19], and that small oxidized entities form during calcination, especially as the Ag loading increased, but the calcination temperature of 600 °C is high enough to make them unstable and reduce them as Ag_n clusters, leading to the SPR absorption band observed at 350 nm (Figure 1A).

It is also interesting to note that the nature of the Ag species also depends on the conditions of calcination, i.e., whether calcination was performed in a muffle furnace under static air [49] or under air or O_2 flow [4]. The speciation also depends on the presence of water in the sample and in the calcination gas. The presence of water on alumina support was shown to favor the formation of hydroxylated Ag species, which was more easily reducible than Ag_2O [7]. Cai and coll. [70] showed that a treatment at 500 °C of 0.08 to 0.44% Ag/SiO_2 under water vapor

favored the reduction of Ag^+ into Ag^0 and the formation of a SPR band at around 400 nm, whereas a treatment in dry air at 500 °C did not lead to any SPR band. The nature of the Ag species also depends on the nature of the support. Bethke and Kung [4] reported that a 6% Ag/Al_2O_3 sample calcined at 700 °C was white and did not show any SPR band while a 6% Ag/SiO_2 sample was beige and showed XRD peaks of Ag^0 which confirmed that Ag is much better dispersed on alumina than on silica after calcination [48].

4.2.2. Comparison with the reduced Ag/Al_2O_3 samples

As mentioned above, $Ag(2.6)/Al_2O_3$, reduced under H_2 at 550 °C became brown, and the SPR band at 420 nm was much stronger and broader (full width at half maximum (FWHM) ~350 nm) (**Figure 2f**) than that of the calcined samples (350 nm and FWHM ~90 nm (**Figures 1 and 2a**). The color compares well with the rust color reported by Bethke et al. [4] for both 2 and 6% Ag/Al_2O_3 samples reduced up to 700 °C, although the SPR band was at 400 nm (**Table 3**) and Ag^0 was detected by XRD. Richter et al. [7] also reported a SPR band around 400 nm when 1 and 5% Ag/Al_2O_3 samples calcined at 500 °C were afterwards *in situ* reduced up to 550 °C (**Table 3**). The SPR bands, which appeared at 100 °C for the 5% Ag and at 300 °C for the 1% Ag samples, were proposed to arise from the reduction of Ag_2O particles, which were larger in the calcined 5% Ag sample than in the 1% Ag one and therefore easier to reduce. Other results from the literature, listed in **Table 3**, also pointed out a band at around 400 nm due to the SPR of Ag^0 nanoparticles in Ag/Al_2O_3 samples thermally reduced in H_2.

4.2.3. Reversibility of the Ag^+/Ag^0 redox phenomenon

Some authors reported the disappearance of the SPR band and the re-oxidation of metallic silver into oxidized silver species and *vice-versa*, i.e., a reversible Ag^+/Ag^0 redox phenomenon, when alternate oxidation/reduction treatments were performed [7, 45, 65, 69] . Keshavaraja et al. [45] showed that the re-calcination of 1.5% Ag/Al_2O_3 at temperature higher than 300 °C led to the disappearance of the SPR band and to the reappearance of a band at 260-350 nm, associated to the reoxidation and redispersion of metallic silver onto the support. These authors also reported the reversibility of the Ag^+/Ag^0 oxidation states in redox cycles. Richter et al. [7] also observed this phenomenon by *in situ* UV-visible spectroscopy during cycles of reduction and calcination of 1% Ag/Al_2O_3 from RT to 550 °C. The same phenomenon was observed for Ag/SiO_2: Pal and De [65] reported that Ag/SiO_2 sample color alternatively changed between yellow (SPR band at 407 nm) after treatment at 450 °C in H_2-N_2 and white (sample bleaching)

after treatment at 450 °C in air, and Cai and coll. [69], added that the SPR absorption was dependent on the Ag loading and on the Ag particle size for a series of 0.12 to 2.4% Ag/SiO_2 samples.

The difference in color, SPR band position and band width after reduction between reduced and calcined Ag/Al_2O_3 samples can be explained by the fact that the Ag^0 particles are larger after reduction (3.7 nm in average, **Figures 4A and S1A**) than after calcination (Ag_n clusters not visible by TEM). Indeed, a SPR red-shift, such as the one from 350 to 420 nm, is expected when the particle size increases [20, 21, 71], and a band broadening, such as the one from 90 to 350 nm, is expected when the size distribution increases, and/or when the particles interact with each other when their density increases [20, 22]. The weaker and narrrower absorption band of the calcined sample, i.e, the smaller surface area of the band, is an indication of a lower proportion of Ag involved in the Ag_n clusters of the calcined sample than in the Ag^0 particles after reduction, confirming that a large fraction of Ag in the calcined samples is present as isolated Ag^+ species.

4.3 Ageing of the calcined Ag/Al_2O_3 catalysts

Now, one can focus on the phenomenon of ageing of the calcined Ag/Al_2O_3 catalysts, i.e., on the possible reasons for the evolution of the color of the samples with time, from white-yellowish to gray-black (**Table 1**) and for the evolution of the Ag plasmon band: higher intensity, red-shift and broadening in the whole visible range (**Figure 1B**). To complement the data of XRD and electron microscopy, photoluminescence and XAS characterizations were also performed. The evolution of the silver state between aged and re-calcined samples were investigated through these two techniques since re-calcination provides samples in a state close to that of samples calcined just after preparation according to color and UV-visible spectra (**Table 1** and **Figure 1**).

4.3.1. Photoluminescence

Photoluminescence is a the technique of choice to detect oxidized isolated or clustered Ag species in a matrix or onto a support [72-76] since metallic silver does not emit photoluminescence. The literature essentially reports on photoluminescence studies of Ag^+ in matrices, such as silica glasses [72-75]. Only a few works deal with supported Ag materials, and no papers on Ag/Al_2O_3 could be found, the closest ones are about Ag in ZSM-5 zeolites

studied by Anpo and coll. [76-78]. Hence, experiments of photoluminescence were carried out on the aged Ag(2.6)/Al$_2$O$_3$ sample and compared to the same sample after re-calcination at 600 °C. The experimental conditions for the photoluminescence study were close to those used by Anpo and coll., i.e., the samples were first evacuated under high vacuum at RT to eliminate adsorbed water and oxygen and avoid Ag$^+$ reduction. The emission spectra were recorded at around 10 K, with an excitation wavelength at 280 nm (see section Experimental). **Figure 5** shows the emission spectra of Ag(2.6)/Al$_2$O$_3$ aged (**spectrum a**) and re-calcined (**spectrum b**) and those of the alumina support used as reference, as such (**spectrum c**) and after calcination at 600 °C (**spectrum d**). The four spectra show thin peaks in addition to the broad emission band between 350 and 600 nm, especially intense for the Ag/Al$_2$O$_3$ samples. The thin peak at 560 nm corresponds to the second harmonic of the excitation spectrum while the other thin peaks at 367, 373 and the broader one at 382 nm are probably due to impurities contained into the alumina. We could check that they cannot be due to iron impurities as the Fe emission is expected at wavelength higher than 600 nm [79].

The emission spectra in the 350-600 nm range are much less intense for the alumina support than those of the Ag(2.6)/Al$_2$O$_3$ samples, aged and re-calcined, respectively, indicating that the strong emission centered at 450 nm of the Ag(2.6)/Al$_2$O$_3$ sample results from the presence of oxidized Ag species. The comparison of the intensities of spectra a and b also shows that Ag(2.6)/Al$_2$O$_3$ contained much more oxidized Ag species after re-calcination than in the aged one. One can therefore infer that the re-calcination of Ag(2.6)/Al$_2$O$_3$ increases the amount of highly dispersed Ag$^+$ species and/or of positively charged Ag$_n$ clusters. *A contrario*, this means that the ageing process reduces their amount because of silver reduction.
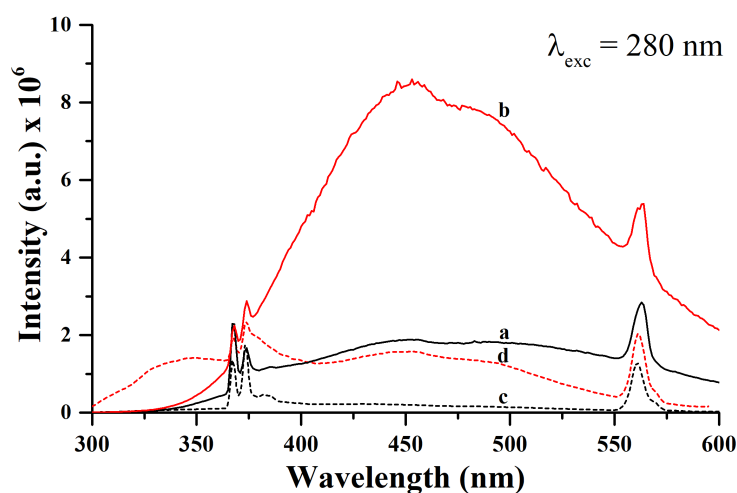

Figure 5: Photoluminescence spectra (λ_{exc} =280 nm) of Ag(2.6)/Al$_2$O$_3$ (a) aged, (b) re-calcined at 600 °C and alumina (doted lines) (c) as such, (d) calcined at 600 °C.

4.3.2. XAS

As for photoluminescence, the XAS experiments at the Ag K-edge were conducted on the aged and re-calcined $Ag(2.6)/Al_2O_3$ samples. Additional information can be found in **Table 4** and **SupInf4**.

Figure 6A shows the XANES spectra of the two samples along with those of the Ag-foil, $AgNO_3$ and Ag_2O references. The $AgNO_3$ spectrum shows a small edge shift of +2.8 eV and a stronger white line intensity compared to the Ag-foil and Ag_2O references (both presenting the same edge at 25514 eV). The XANES spectra of aged $Ag(2.6)/Al_2O_3$ and re-calcined $Ag(2.6)/Al_2O_3$ are roughly similar, and look "intermediate" between those of $AgNO_3$ and Ag-foil. However, the one of the re-calcined sample shows a slightly stronger white line intensity and a small edge shift of +0.4 eV (25515.7 eV for the aged compared to 25516.1 eV for the re-calcined sample), suggesting the presence of a higher proportion of Ag^+ after calcination.

The Fourier-transforms of the EXAFS signals (**Figure 6B**) reveal two types of Ag neighbors in both the aged and the re-calcined $Ag(2.6)/Al_2O_3$ samples: one in the 1-2 Å region and one in the 2-3 Å region. One can note that the relative intensity of the two peaks is different according to the sample, with a relatively more intense second peak for the aged sample. In addition, the first peak of the aged sample is shifted to slightly larger distance. EXAFS fitting (see also **SupInf6**) indicates that the first peak is due to the contribution of two backscattering paths, the Ag-O path with a small contribution due to Ag-Ag path while the second peak is solely comprised of one Ag-Ag backscattering path characteristic of Ag^0.

From the Fourier-transforms of the EXAFS signals (**Figure 6B**) and the EXAFS parameters obtained by EXAFS fitting (**Table 4**), one can propose that the two samples contain two types of Ag species:

- Ag^+ species, since the first peak mainly fits with Ag-O backscattering with distances of 2.26 Å for the aged sample and 2.27 Å for the re-calcined one. This distance is intermediate between those of Ag-O in Ag_2O (2.048 Å) and $AgAlO_2$ (2.354 Å) (**SupInf6**), and could correspond to Ag-O bonds of Ag-O-Al species. The small number of oxygen neighbors, close to 1 for both $Ag(2.6)/Al_2O_3$ samples, suggests that the Ag^+ species are highly dispersed on the alumina support in the form of single atoms or small clusters.

- Ag^0 species since the second peak fits with Ag-Ag backscattering distances of 2.84 and 2.81 Å for the aged and the re-calcined samples, respectively, which are closer to those of bulk silver metal (2.889 Å) than to those in Ag_2O (3.345 Å) and $AgAlO_2$ (3.214 Å) (**SupInf6**). The small number of Ag neighbors (3 and 2 for the aged and the re-calcined samples, respectively)

indicates the presence of very small Ag particles in both samples. The smaller Ag-Ag distance compared to that of bulk silver likely results from the small size of the particles. Similar contraction of the metal-metal distance compared to bulk has been observed in several cases of supported Ag samples after reduction [17, 18, 80]. It can be mentioned that in the case of Au nanoparticles, a direct correlation was established between the size of the Au^0 particles and the extent of the contraction of the Au-Au distances [81].

The XAS results obtained for the re-calcined sample are not very different from those of the literature obtained for various freshly calcined Ag/Al_2O_3 samples of close Ag loadings (**Table 4**): most works report Ag-Ag contributions with low coordination numbers and comparable distances.

The slightly larger number of Ag neighbors and smaller number of O neighbors in the aged sample than in the re-calcined sample indicate the presence of larger Ag^0 particles. This is consistent with the relatively larger contribution of the Ag-Ag component for the aged sample (**Figure 6B**), i.e., the presence of a higher proportion of Ag^0 in the sample, due to the reduction of part of Ag^+ species into Ag^0 during aging. Note that the presence of a smaller number of Ag neighbors in the re-calcined sample than in the aged sample is consistent with the presence of small Ag_n clusters already attested by the presence of the UV band at 350 nm in **Figure 1C**. One cannot observe substantial increase in the peak intensity of the Ag-O contribution of the re-calcined sample (**Figure 6B**) with respect to the aged one (**Figure 6A**), even though there is a two-fold increase in the Ag-O coordination number, from 0.6 to 1.2. This is due to the simultaneous increase in the Debye-Waller factor, revealing that the redispersion of the silver atoms introduces some disorder in the system. What is more puzzling is why the number of Ag neighbors remains small in the aged sample and much smaller than the values expected considering the size of the Ag particles measured by TEM. Since the number of Ag neighbors determined by EXAFS is an average value, an explanation could be that Ag^0 particles coexist with Ag_n clusters and that their proportion is low and contribute to only a small increase in the number of Ag neighbors. The quantitative results must be anyway considered with care since the X-ray beam of third generation synchrotron may have an impact on the samples, participating to the reduction of Ag^+ in the aged and re-calcined samples. The important result brought by these XAS experiments is that it supports the photoluminescence results indicating the formation of Ag^0 during ageing.
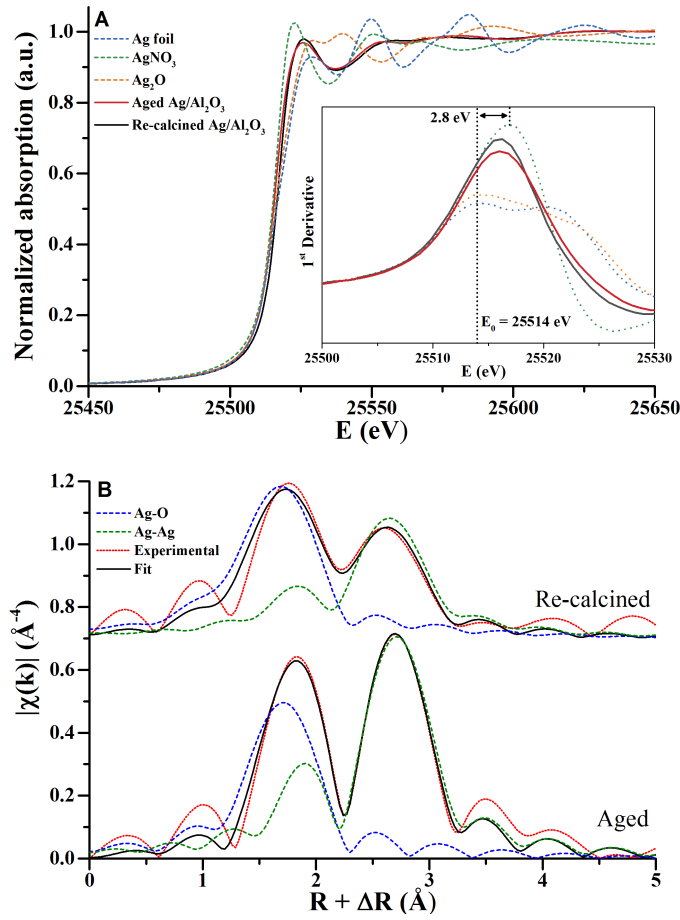
Figure 6: (**A**) XANES at the Ag threshold of Ag(2.6)/Al$_2$O$_3$ (a) aged (red), (b) re-calcined at 600 °C (black), and references: Ag foil (dotted blue), AgNO$_3$ (dotted green), Ag$_2$O (dotted red); (**B**) Ag K-edge (non phase corrected) $\chi(R)$ in R^3 space (red) and fittings components (real part) of Ag(2.6)/Al$_2$O$_3$ sample, aged (bottom) and re-calcined at 600 °C (top).

Table 4: Fitting parameters of the EXAFS at the Ag-K edge for the aged and re-calcined Ag(2.6)/Al$_2$O$_3$ samples (Δk = 3.3 - 9.0 Å^{-1}, Δr = 1.4-3.5 Å, S$_0$ = 0.82).

Sample	Path/shell	R (Å)	Coordination number	σ^2 (10^{-3} Å^2)	ΔE (eV)	R factor (%)	ref
Aged Ag/Al$_2$O$_3$	Ag-O	2.26 ± 0.01	0.6 ± 0.2	5 ± 3	-0.1	0.31	This work
	Ag-Ag	2.84 ± 0.01	2.9 ± 0.4	21 ± 2			
Re-calcined Ag/Al$_2$O$_3$	Ag-O	2.27 ± 0.01	1.2 ± 0.3	14 ± 3	-3.0	0.48	
	Ag-Ag	2.81 ± 0.01	2.2 ± 0.4	25 ± 3			
Calcined 2%Ag/Al$_2$O$_3$	Ag-O	2.35	1.6	4.8		42.1	[18]
	Ag-Ag	2.80	0.8	5.1			
Calcined 2%Ag/Al$_2$O$_3$	Ag-O	2.48	4.4			4.9	[11]
	Ag-Ag	2.74	0.6				
Calcined 5%Ag/Al$_2$O$_3$	Ag-O	2.21	1.72	2.7		26.9	[80]
	Ag-Ag	2.66	2.37	6.2			
Calcined 1%Ag/Al$_2$O$_3$	Ag-O	2.5 (0.1)	2.6 (0.5)	11	6.0	0.95	[88]
	Ag-Ag						
Calcined 2%Ag/Al$_2$O$_3$	Ag-O	2.4 (0.1)	2.6 (1.3)	28	-2.4	0.67	
	Ag-Ag	2.7 (0.1)	1.3 (0.7)	23	-10.6		
Calcined 5%Ag/Al$_2$O$_3$	Ag-O	2.3 (0.1)	1.9 (0.2)	23	-6.6	1.51	
	Ag-Ag	2.7 (0.1)	1.5 (0.4)	24	-7.3		

4.4. Discussion on the mechanism of Ag/Al$_2$O$_3$ ageing

At this step, we know that the calcined Ag/Al$_2$O$_3$ samples contain isolated Ag$^+$ ions and Ag$_n$ clusters (<1 nm), responsible for the yellowish color in the most highly loaded samples, that the aged samples contain Ag^0 aggregates and nanoparticles, and that less Ag$^+$ and more Ag^0 are present in the aged samples than in the calcined ones, according to photoluminescence and XAS. Hence, these results indicate the reduction of Ag$^+$ into Ag^0 and the formation of Ag^0 particles during ageing; the ageing process is all the more efficient and faster that the samples are exposed to ambient air and light, and that the Ag loading is high.

The review reported at the beginning of the paper focused on the possible reasons for changes in the optical properties of materials containing metallic Ag^0 particles. However, the ageing process of Ag/Al$_2$O$_3$ samples must also include a step of reduction of Ag$^+$ species initially present in the calcined samples.

The literature data gathered in this review showed that some Ag$^+$-containing compounds are intrinsically photo-sensitive and do not require a semiconducting oxide support to reduce under ambient air. Ag$_2$O is a p-type semiconducting oxide of brown color with a bandgap of ~1.3 eV (955 nm), and it is photo-sensitive and unstable under light exposure: it decomposes into Ag^0 through the intermediate formation of AgO (in fact, an oxide described as a mixture of Ag$_2$O and Ag$_3$O$_2$), which is also unstable at ambient temperature, and readily photo-reduces into metallic Ag and O$_2$:

$$Ag_2O \rightarrow AgO + Ag$$
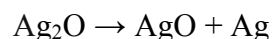
$$AgO \rightarrow Ag + 1/2\ O_2 \tag{Equation 1}$$

Ag$^+$ in silver halide is also photo-sensitive, and reduces into Ag^0; this reaction is at the origin of the formation of the latent image in silver photography [82]. Ag$^+$ dispersed on TiO$_2$ films can also photo-reduce into Ag^0 particles, but TiO$_2$ can also be involved in the reaction [83].

Ag$^+$ auto-reduction has also been reported in the literature. One example concerns Ag$^+$ auto-reduction of AgNaA-zeolites during TPD [84]. As the TPD proceeded, the sample initially white, turned to deep yellow, then red, and released oxygen. The overall stoichiometry of the reaction was proposed to be:

$$2(Ag^+ZO^-) -> 1/2O_2 + Ag_2^0 + ZO^- + Z^+,$$
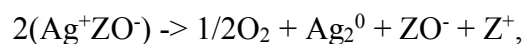
where ZO$^-$ represents the zeolite lattice and Z$^+$ a Lewis acid site. Ag$^+$ auto-reduction was also found to occur at the surface of hydroxyapatites (Hap) when a AgSO$_4$ solution (colorless) was put in contact with HAp [85]; depending on the Ag concentration, the suspension turned pale yellow or purple.

One can therefore propose that auto-reduction occurs during the ageing process of the Ag/Al$_2$O$_3$ samples. In addition to auto-reduction, a mechanism of photo-reduction can certainly also occur. For instance, after the UV-Visible and XRD experiments, the beam impact let a darker spot at the surface of the samples squeezed in their sample holders; this was especially visible on calcined samples because of their pale color. XAS is also suspected to induce Ag$^+$ reduction. The fact that sample darkening also occurred when the samples were stored in a desiccator in dark, but less rapidly than in ambient air, is attributed to auto-reduction, but one cannot discard the fact that the samples had been exposed to air and light during a short period after calcination and before storage, which may have initiated phot-reduction.

Hence, one can proposed that the **first step** of the ageing process of the Ag/Al$_2$O$_3$ samples is a gradual photo- and/or auto-reduction of Ag$^+$ species into Ag^0, followed by the growth of Ag^0 particles. Since the ageing process was all the more efficient that the Ag loading was high, it is possible that the reduction of Ag$^+$ was facilitated by the presence of the Ag$_n$ clusters, that could act as nucleation sites for the growth of Ag^0 particles. Then, based on the data of the review in **Section 2.1** on the influence of size and aggregation degree of Ag^0 particles on the optical properties (), one can propose that the **second ageing step** is the aggregation of Ag^0 species or of small NPs formed during from the first step, and the formation of larger particles aggregates. The presence of small NPs and large aggregates (30-50 nm) in the aged Ag/Al$_2$O$_3$ samples (**Figure 4B)** indicates that migration of Ag species occurs. Such a phenomenon was attested in the case of 75 nm PVP-stabilized Ag^0 NPs supported on a silica substrate, which were exposed to ambient air with humidity $\geq$50% [39]. After one-week exposure, new small particles (5-10 nm and smaller) were visible by TEM in the immediate vicinity of large Ag^0 particles. Their number increased after weeks, and spread in larger areas around the parent particles. A three-stage mechanism was proposed by the authors: (1) surface oxidation with ambient oxygen and adsorbed water; (2) ion silver diffusion away from the parent particle in the adsorbed water layer driven by the concentration gradient (3) nucleation and growth of new particles via chemical and/or photochemical reduction of silver ion on the surface.

Finally, a **third ageing step** must be considered because once the Ag^0 particles were formed, their surface could be altered as reported in **Section 2.2** for bulk silver artifacts and Ag^0 particles in contact with ambient air. According to Pelaez et al. [33], Ag^0 particles on alumina preferentially react with O$_2$ in the presence of humidity rather than with S-compounds in air; this could explain why sulfur was not detected in our samples by XPS and X-EDS,

however AgO_x was not detected either. In contrast, formation of silver carbonates was attested by XRD and only on samples with rather high Ag loadings (3.5 and 4.1 %) (**Figure 3**). Although their presence was unexpected since according to literature, silver carbonates were detected only in very specific atmospheres (in high altitude with enhanced UV light [36] or under humid O_2 in the presence or absence of UV light [37]), one must postulate that their presence is the result of sample alteration. However, one cannot affirm that they are located on Ag^0 particle surfaces. Indeed, it is difficult to conceive that a surface layer of carbonates could be detected by XRD, whereas the Ag^0 core of the particles are not detected; moreover silver carbonates were not either detected on the aggregates analyzed by HRTEM. Note that by X-EDS, it is not possible to discriminate carbon of silver carbonate from carbon of the carbon membrane of the copper grid and from the carbon of contamination generated under beam exposure.

5. Conclusion

This work addressed the issue of the color of calcined Ag/Al_2O_3 catalysts which depends on the Ag loading and that of their further color evolution when the samples are stored in ambient air or in a desiccator and in dark. The calcined samples were initially white or yellowish depending on the Ag loading. On the basis of literature data and a characterization study involving several techniques, the conclusion is that the freshly calcined Ag/Al_2O_3 samples contain isolated Ag^+ species (UV bands at 210 and 230 nm) and Ag_n clusters (<1 nm, neutral or slightly positively charged) whose proportion increases with the Ag loading; the presence of these clusters is responsible for the plasmon band at ~350 nm and for the yellowish color of the Ag/Al_2O_3 samples containing more than 2 % Ag. These results can be used to complete a scheme proposed earlier in our catalytic study on C_3H_6-SCR of NO_x [3, 19] using the same Ag/Al_2O_3 samples. The NO_x-TPD method developed by Thomas and coll. [42] was used to evaluate the Ag dispersion of the same series of calcined Ag/Al_2O_3 samples (NO_x species adsorb only onto the alumina support). The plateau of NO_x uptake observed for the Ag loadings larger than 2 % (**Figure 7**) can now be attributed more specifically to the presence of Ag_n clusters and not to Ag_2O clusters as anticipated earlier.

The calcined Ag/Al_2O_3 catalysts gradually turned gray/black during storage with a rate that depended on whether the samples were stored in air or under vacuum, in the absence of light or not. The color changes were accompanied by a red-shift, broadening and increasing intensity of the plasmon band, and the most highly loaded samples darkened faster. This ageing process was discussed on the basis of the results of characterization of aged samples and of data of the literature. Sample darkening during ageing was correlated with a modification of the nature of

the Ag phase, i.e., with the reduction of Ag^+ species accompanied by Ag migration and the formation of Ag^0 particles and aggregates. The Ag_n clusters, already present after calcination, may act as nucleation sites for the growth of Ag^0 particles. For sample aging in air and light, photo-reduction may occur in addition to auto-reduction and for ageing in vacuum and in dark, auto-reduction is certainly the main reduction mechanism.

Finally, it can be anticipated that the absence of reports concerning ageing of supported Ag catalysts results from the fact that the ageing process is reversible; when a re-calcination treatment is applied, the catalyst recovers its initial color and UV-visible spectrum. In addition, in the studies on $deNO_x$ reactions over these catalysts, the NO_x species and especially NO_2 (more oxidizing than oxygen as shown in the paper), may still be more efficient than calcination to re-disperse Ag of aged Ag/Al_2O_3 samples.
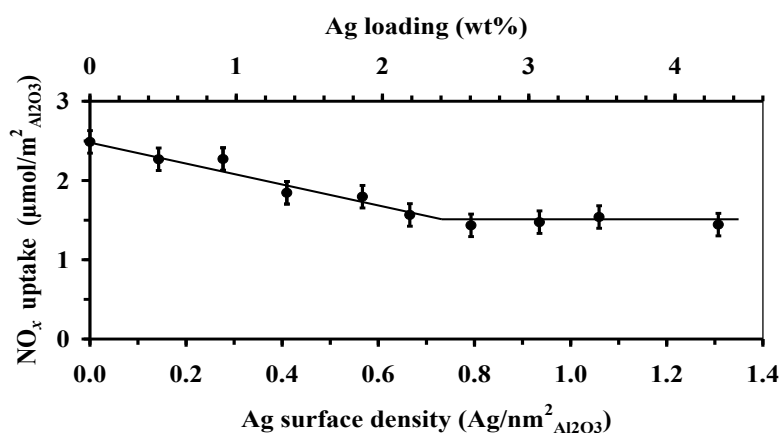

Figure 7: Evolution of the NO_x uptake during the NO_x-TPD of calcined Ag/Al_2O_3 samples as a function of the Ag loading according to ref. [3].

References

1. R. Burch, Catal. Rev. **46**, 271-334 (2004)

2. H. He, X. Zhang, Q. Wu, C. Zhang and Y. Yu, Catal. Surv. Asia **12**, 38-55 (2008)

3. T. Chaieb, L. Delannoy, C. Louis and C. Thomas, Appl. Catal., B **142–143**, 780-784 (2013)

4. K.A. Bethke and H.H. Kung, J. Catal. **172**, 93-102 (1997)

5. K. Arve, L. Capek, F. Klingstedt, K. Eranen, L.E. Lindfors, D.Y. Murzin, J. Dedecek, Z. Sobalik and B. Wichterlova, Top. Catal. **30-31**, 91-95 (2004)

6. N. Bogdanchikova, F.C. Meunier, M. Avalos-Borja, J.P. Breen and A. Pestryakov, Appl. Catal., B **36**, 287-297 (2002)

7. M. Richter, A. Abramova, U. Bentrup and R. Fricke, J. Appl. Spectrosc. **71**, 400-403 (2004)

8. K. Shimizu, J. Shibata, H. Yoshida, A. Satsuma and T. Hattori, Appl. Catal., B **30**, 151-162 (2001)

9. K. Shimizu, T. Higashimata, M. Tsuzuki and A. Satsuma, J. Catal. **239**, 117-124 (2006)

10. X. She and M. Flytzani-Stephanopoulos, J. Catal. **237**, 79-93 (2006)

11. K. Shimizu, M. Tsuzuki, K. Kato, S. Yokota, K. Okumura and A. Satsuma, J. Phys. Chem. C **111**, 950-959 (2007)

12. N.A. Sadokhina, A.F. Prokhorova, R.I. Kvon, I.S. Mashkovskii, G.O. Bragina, G.N. Baeva, V.I. Bukhtiyarov and A.Y. Stakheev, Kinet. Catal. **53**, 107-116 (2012)

13. P. Granger and V.I. Parvulescu, Chem. Rev. **111**, 3155-3207 (2011)

14. P.G. Savva and C.N. Costa, Catal. Rev. - Sci. Eng. **53**, 91-151 (2011)

15. V.I. Bukhtiyarov and A. Knop-Gericke, RSC Nanosci. Nanotechnol. **19**, 214-247 (2011)

16. K.C. Waugh and M. Hague, in Mechanisms in Homogeneous and Heterogeneous Epoxidation Catalysis, Edited by S. T. Oyama, Elsevier, 233-263 (2008)

17. K. Shimizu and A. Satsuma, J. Jpn. Pet. Inst. **54**, 347-360 (2011)

18. J.P. Breen, R. Burch, C. Hardacre and C.J. Hill, J. Phys. Chem. B **109**, 4805-4807 (2005)

19. T. Chaieb, L. Delannoy, G. Costentin, C. Louis, S. Casale, R.L. Chantry, Z.Y. Li and C. Thomas, Appl. Catal., B **156-157**, 192-201 (2014)

20. E. Cottancin, M. Broyer, J. Lerme and M. Pellarin, Optical Properties of Metal Clusters and Nanoparticles, Edited by Sattler, Klaus D, Handbook of Nanophysics **6**, 24-21/24-25 (2011)

21. F.M. Kelly and J.H. Johnston, ACS Appl. Mater. Interfaces **3**, 1083-1092 (2011)

22. G. Carotenuto and F. Nicolais, Mater. **2**, 1323-1340 (2009)

23. B. Ritzer, M.A. Villegas and J.M. Fernandez Navarro, J. Sol-Gel Sci. Technol. **8**, 917-921 (1997)

24. J.D. Sinclair, J. Electrochem. Soc. **129**, 33-40 (1982)

25. J.P. Franey, G.W. Kammlott and T.E. Graedel, Corros. Sci. **25**, 133-143 (1985)

26. T.E. Graedel, J.P. Franey, G.J. Gualtieri, G.W. Kammlott and D.L. Malm, Corros. Sci. **25**, 1163-1180 (1985)

27. H.E. Bennett, R.L. Peck, D.K. Burge and J.M. Bennett, J. Appl. Phys. **40**, 3351-3360 (1969)

28. M.D. Mcmahon, R. Lopez, H.M. Meyer, L.C. Feldman and R.F. Haglund, Appl. Phys. B **80**, 915-921 (2005)

29. W. Cao and H.E. Elsayed-Ali, Mater. Lett. **63**, 2263-2266 (2009)

30. L. Wang, W. Xiong, Y. Nishijima, Y. Yokota, K. Ueno, H. Misawa, G. Bi and J. Qiu, Opt. Express **19**, 10640-10646 (2011)

31. G. Baraldi, M. Carrada, J. Toudert, F.J. Ferrer, A. Arbouet, V. Paillard and J. Gonzalo, J. Phys. Chem. C **117**, 9431-9439 (2013)

32. A. Andrieux-Ledier, B. Tremblay and A. Courty, Langmuir **29**, 13140-13145 (2013)

33. R.J. Pelaez, A. Castelo, C.N. Afonso, A. Borras, J.P. Espinos, S. Riedel, P. Leiderer and J. Boneberg, Nanotechnology **24**, 365702-365708 (2013)

34. Z.Y. Chen, D. Liang, G. Ma, G.S. Frankel, H.C. Allen and R.G. Kelly, Corros. Eng., Sci. Technol. **45**, 169-180 (2010)

35. S. Capelo, P.M. Homem, J. Cavalheiro and I.T.E. Fonseca, J. Solid State Electrochem. **17**, 223-234 (2013)

36. C.E. Sanders, D. Verreault, G.S. Frankel and H.C. Allen, J. Electrochem. Soc. **162**, C630-C637 (2015)

37. R. Wiesinger, M. Schreiner and C. Kleber, Appl. Surf. Sci. **256**, 2735-2741 (2010)

38. T. Graedel, J. Electrochem. Soc. **139**, 1963-1970 (1992)

39. R.D. Glover, J.M. Miller and J.E. Hutchison, ACS nano **5**, 8950-8957 (2011)

40. X. Wang, C. Santschi and O.J. Martin, Small **13**, 1700044 (2017)

41. M. Kesim, H. Yu, Y. Sun, M. Aindow and S. Alpay, Corrosion Science **135**, 12-34 (2018)

42. H.Y. Law, J. Blanchard, X. Carrier and C. Thomas, J. Phys. Chem. C **114**, 9731-9738 (2010)

43. E. Sayah, D. Brouri, Y. Wu, A. Musi, P. Da Costa and P. Massiani, Appl. Catal., A **406**, 94-101 (2011)

44. B. Ravel and M. Newville, J. Synchr. Rad. **12**, 537-541 (2005)

45. A. Keshavaraja, X. She and M. Flytzani-Stephanopoulos, Appl. Catal., B **27**, L1-L9 (2000)

46. J. Texter, J.J. Hastreiter and J.L. Hall, J. Phys. Chem. **87**, 4690-4693 (1983)

47. M. Richter, U. Bentrup, R. Eckelt, M. Schneider, M.M. Pohl and R. Fricke, Appl. Catal., B **51**, 261-274 (2004)

48. A.N. Pestryakov and A.A. Davydov, J. Electron. Spectrosc. Relat. Phenom. **74**, 195-199 (1995)

49. E. Aneggi, J. Llorca, C. de Leitenburg, G. Dolcetti and A. Trovarelli, Appl. Catal., B **91**, 489-498 (2009)

50. J. Shibata, Y. Takada, A. Shichi, S. Satokawa, A. Satsuma and T. Hattori, J. Catal. **222**, 368-376 (2004)

51. Z. Li and M. Flytzani-Stephanopoulos, J. Catal. **182**, 313-327 (1999)

52. K. Sato, T. Yoshinari, Y. Kintaichi, M. Haneda and H. Hamada, Appl. Catal., B **44**, 67-78 (2003)

53. A.N. Pestryakov, A.A. Davydov and L.N. Kurina, Russ. J. Phys. Chem. (Engl. Transl.) **60**, 2081 (1986)

54. J. Michalik, J. Sadlo, T. Kodaira, S. Shimomura and H. Yamada, J. Radioanal. Nucl. Chem. **232**, 135-138 (1998)

55. G.A. Ozin and H. Huber, Inorg. Chem. **17**, 155-163 (1978)

56. G.A. Ozin, F. Hugues, S.M. Mattar and D.F. McIntosh, J. Phys. Chem. **87**, 3445-3450 (1983)

57. P. Mulvaney and A. Henglein, J. Phys.l Chem. **94**, 4182-4188 (1990)

58. B. Ershov, E. Janata, A. Henglein and A. Fojtik, J. Phys.l Chem. **97**, 4589-4594 (1993)

59. E. Gachard, J. Belloni and M.A. Subramanian, J. Mater. Chem. **6**, 867-870 (1996)

60. B.G. Ershov, E. Janata and A. Henglein, J. Phys. Chem. **97**, 339-343 (1993)

61. S. Fedrigo, W. Harbich and J. Buttet, Phys. Rev. B: Condens. Matter **47**, 10706-10715 (1993)

62. J. Tiggesbaeumker, L. Koeller, K.H. Meiwes-Broer and A. Liebsch, Phys. Rev. A **48**, R1749-R1752 (1993)

63. H. Abe, K.P. Charle, B. Tesche and W. Schulze, Chem. Phys. **68**, 137-141 (1982)

64. A. Henglein, Isr. J. Chem. **33**, 77-88 (1993)

65. S. Pal and G. De, Mater. Res. Bull. **44**, 355-359 (2009)

66. S.P. Ramnani, S. Sabharwal, J.V. Kumar, K.H.P. Reddy, K.S.R. Rao and P.S.S. Prasad, Catal. Commun. **9**, 756-761 (2008)

67. T. Nakatsuji, R. Yasukawa, K. Tabata, K. Ueda and M. Niwa, Appl. Catal., B **17**, 333-345 (1998)

68. R.C. Weast, CRC Handbook of Chemistry and Physics, 70th ed., CRC Press, Boca Raton, FL, p. D-43

69. H. Bi, W. Cai, C. Kan, L. Zhang, D. Martin and F. Trager, J. Appl. Phys. **92**, 7491-7497 (2002)

70. Y. Gan, W. Cai, G. Fu and J. Hu, J. Phys.: Condens. Matter **16**, L201-L206 (2004)

71. R. Patakfalvi, D. Diaz, D. Velasco-Arias, G. Rodriguez-Gattorno and P. Santiago-Jacinto, Colloid. Polym. Sci. **286**, 67-77 (2008)

72. A. Meijerink, M.M.E. van Heek and G. Blasse, J. Phys. Chem. Solids **54**, 901-906 (1993)

73. E. Borsella, E. Cattaruzza, G. De Marchi, F. Gonella, G. Mattei, P. Mazzoldi, A. Quaranta, G. Battaglin and R. Polloni, J. Non-Crystal. Solids **245**, 122-128 (1999)

74. S.E. Paje, Garcı, x, M.A. a, J. Llopis and M.A. Villegas, J. Non-Crystal. Solids **318**, 239-247 (2003)

75. J.A. Jiménez, M. Sendova, T. Hartsfield and M. Sendova-Vassileva, Mater. Res. Bull. **46**, 158-165 (2011)

76. M. Matsuoka, W.-S. Ju, H.-J. Chen, Y. Sakatani and M. Anpo, Res. Chem. Interm. **29**, 477-483 (2003)

77. M. Anpo, M. Matsuoka, H. Mishima and H. Yamashita, Res. Chem. Interm. **23**, 197-217 (1997)

78. S.M. Kanan, M.A. Omary, H.H. Patterson, M. Matsuoka and M. Anpo, J. Phys. Chem. B **104**, 3507-3517 (2000)

79. V.O. Stoyanovskii and V.N. Snytnikov, Kinet Catal. **50**, 450-455 (2009)

80. S.T. Korhonen, A.M. Beale, M.A. Newton and B.M. Weckhuysen, J. Phys. Chem. C **115**, 885-896 (2010)

81. J. Miller, A. Kropf, Y. Zha, J. Regalbuto, L. Delannoy, C. Louis, E. Bus and J.A. van Bokhoven, J. Catal. **240**, 222-234 (2006)

82. J. Belloni, Radiat. Phys. Chem. **67**, 291-296 (2003)

83. K. Kawahara, K. Suzuki, Y. Ohko and T. Tatsuma, Phys. Chem. Chem. Phys. **7**, 3851-3855 (2005)

84. P.A. Jacobs, J.B. Uytterhoeven and H.K. Beyer, J. Chem. Soc., Faraday Trans. 1 **75**, 56-64 (1979)

85. S.K. Arumugam, T.P. Sastry, B. Sreedhar and A.B. Mandal, J. Biomed. Mater. Res. A **80A**, 391-398 (2007)

86. M.K. Kim, P.S. Kim, J.H. Baik, I.-S. Nam, B.K. Cho and S.H. Oh, Appl. Catal., B **105**, 1-14 (2011)

87. B. Inceesungvorn, J. López-Castro, J.J. Calvino, S. Bernal, F.C. Meunier, C. Hardacre, K. Griffin and J.J. Delgado, Appl. Catal., A **391**, 187-193 (2011)

88. H. Deng, Y. Yu, F. Liu, J. Ma, Y. Zhang and H. He, ACS Catal. **4**, 2776-2784 (2014)

Supplementary Material

SupInf1: Other characterization techniques

Despite the risk of thermal reduction of Ag^+ species without H_2 consumption, TPR/TPO experiments were performed. No H_2 or O_2 consumption could be recorded in these samples, even in the optimized conditions recommended in earlier studies, e.g. in TPRs performed after *in situ* pretreatment at 200 °C for 1 h under O_2 [1] and an inert gas [2]. XPS measurements were also performed on a calcined $Ag(3.5)/Al_2O_3$ sample and an aged one, using an Omicron (ESCA+) spectrometer with an Al Kα (hν = 1486.6 eV) X-ray source powered at 14 kV and 20 mA. The XPS peaks were too broad to allow the determination of silver oxidation states. Indeed, the alumina support broadens the silver peaks, and in addition, the assignment of the binding energies is stilla matter of discussion in the literature due to large discrepancy in the values of the Ag3d BE for a given oxidation state provided by the literature [3-6]. The only reliable result obtained was the absence of sulfur detected in the aged samples. The Auger parameter, which was supposed to allow to discriminate Ag^0 from the other oxidation states, however, did not appear meaningful according to a former study [6].

[1] P.S. Kim, M.K. Kim, B.K. Cho, I.-S. Nam, S.H. Oh, J. Catal., 301 (2013) 65-76.
[2] M. Richter, U. Bentrup, R. Eckelt, M. Schneider, M.M. Pohl, R. Fricke, Appl. Catal., B, 51 (2004) 261-274.
[3] X. She, M. Flytzani-Stephanopoulos, J. Catal., 237 (2006) 79-93.
[4] N.A. Sadokhina, A.F. Prokhorova, R.I. Kvon, I.S. Mashkovskii, G.O. Bragina, G.N. Baeva, V.I. Bukhtiyarov, A.Y. Stakheev, Kinet. Catal., 53 (2012) 107-116.
[5] M. Richter, M. Langpape, S. Kolf, G. Grubert, R. Eckelt, J. Radnik, M. Schneider, M.M. Pohl, R. Fricke, Appl. Catal., B, 36 (2002) 261-277.
[6] A.M. Ferraria, A.P. Carapeto, A.M. Botelho do Rego, 86 (2012) 1988-1991.

SupInf2: XRD

Table: Other silver and aluminum compounds whose XRD peaks (in blue) do not match with any of the XRD peaks appearing during ageing of $Ag(4.1)/Al_2O_3$ sample

| Compound - JCPS# - quality - intensities reported	XRD peaks: 2θ - intensity
silver chloride (AgCl) 31-1238 (high) I>50	27.8 (I=50), 32.2 (I=100), 46.2
silver sulfate (Ag_2SO_4) 27-1403 (high) main peaks I≥30	28.1 (I=70), 31.1 (I=100), 33.9 (I= 90), 37.1 (I= 30), 47.2 (I= 30)
silver sulfite (Ag_2SO_3) 23-0644 (indexed) main peaks (I≥80)	14.5 (I=90), 22.3 (I=90), 29.3, 29.8, 30.1, 30.4 (I=100), 31.8, 32.2, 36.1(I=100)
basic carbonate ($AgOHAg_2CO_3$, not found) $Ag_7O_8CO_3$ 53-1292 (high) (I>60)	31.6 (I=100), 52.7 (I=67), 62.7
Silver aluminate α-$AgAlO_2$ (21-1069) (questionable) (I≥60)	14.5 (I=94), 29.2 (I=55), 36.5 (I=100)
Boehmite (AlO(OH) 83-2384 (calculated) (I≥36)	14.5 (I=100), 28.2 (I=36)

SupInf3: TEM
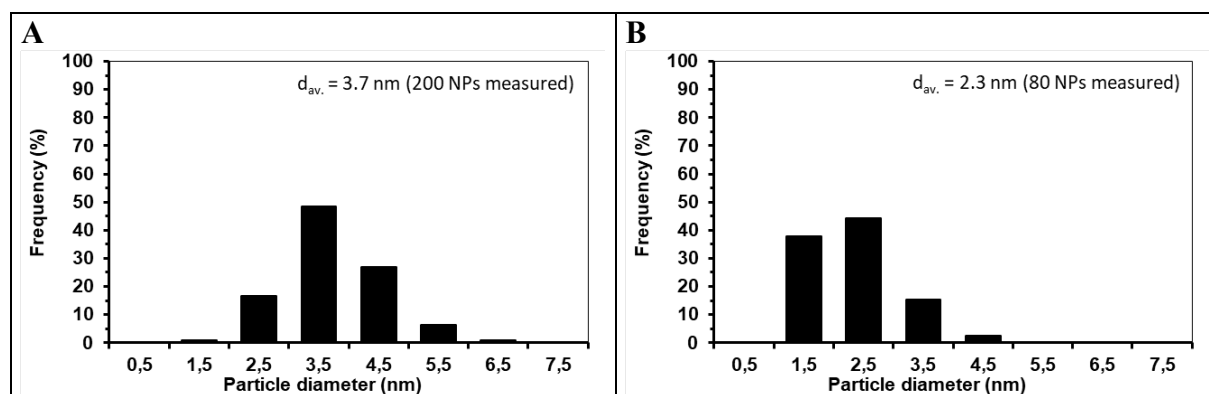
Figure: particle sizes distributions measured from TEM micrographs of (A) 12-month aged Ag(2.6)/Al$_2$O$_3$ then reduced at 550 °C and (B) of small particles in 12-month aged Ag(2.6)/Al$_2$O$_3$ (from micrographs of large magnification as in Figure 4Bb)).

SupInf4: X-EDS

Table: X-EDS measurements performed on aged Ag(4.1)/Al$_2$O$_3$ in areas containing aggregates and in areas containing no visible particles (see Figure below)

Selected areas	O (at.%)	Al (at.%)	Ag (at.%)	S (at.%)
Ag aggregates (see Figure S2)	43.5	13.0	42.5	1.0
	45.5	17.0	37.0	0.5
	45.0	15.0	39.0	1.0
	39.0	5.5	54.5	1.0
	38.0	4.0	57.5	0.5
Areas with no visible Ag NPs	60.0	39.5	0.5	<0.1
	60.0	37.5	1.5	1

Notes: The amount of S is very low, and is found in all areas whether Ag is present or not.
It is not possible to discriminate carbon of possible silver carbonate from carbon of the carbon membrane of the copper grid and of the contamination generated under beam exposure.
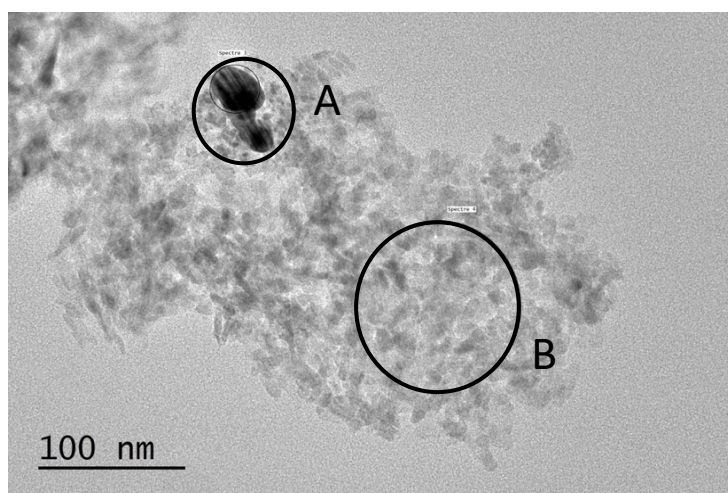

Figure: Example of X-EDS measurements in areas containing Ag aggregates (A) and in areas with no visible Ag NPs (B).

SupInf5: HRTEM

Table A: d-spacings measured by HRTEM on 13 silver nanoparticles and on 43 silver aggregates in aged Ag(4.1)/Al$_2$O$_3$ in aged Ag(3)/Al$_2$O$_3$ and comparison with JCPDS references of Ag compounds (distance, intensity and indexation)

Silver nanoparticles d(Å)	Number of NPs	Silver aggregates d(Å)	Number of aggregates	Ag^0 65-2871 (indexed) d(Å) I hkl	Ag_2O 41-1104 (high) d(Å) I hkl	Ag_2S acanthite * 14-0072 (high) d(Å) I hkl	Monoclinic $AgCO_3$ * 26-0339 (high) d(Å) I hkl	Hexagonal α-Ag_2CO_3 31-1237 (high) d(Å) I hkl	Hexagonal β-Ag_2CO_3 31-1236 (high) d(Å) I hkl	Ag_2SO_4 * 27-1403 (high) d(Å) I hkl	Ag_2SO_3 * 23-0644 (indexed) d(Å) I hkl	AgCl 31-1238 (high) d(Å) I hkl
		1.4	3	1.44 24 220	1.43 8 311							
					1.67 13 220			1.53 16 411 1.87 25 221	1.53 16 330 1.87 16 222	1.67 12 313 1.71 17 062 1.92 12 511 1.93 30 351		1.60 16 222 1.67 16 311
		1.9	2									
2.0	1	2.0	11	2.04 46 200		1.96 20 -123 2.00 16 -131 2.05 16 103 2.07 16 023 2.08 45 200 2.09 16 122	1.98 10 -201				2.10 40 -214 2.12 60 122	1.96 50 220
		2.1	6									
		2.2	3			2.21 45 031	2.16 11 220				2.20 60 130 2.21 90 -213	
2.3	12	2.3	7	2.35 100 111	2.36 28 200		2.28 35 031 2.32 14 121	2.27 16 220			2.25 60 -132 2.27 60 -124 2.29 40 -131 2.30 80 014	
		2.35	3									
		2.4	2			2.38 75 -103 2.42 60 013 2.44 80 121	2.38 13 -121 2.39 11 040			2.42 30 331	2.39 60 112 2.47 80 121 2.49 100 023 2.51 60 102	
		2.5	4			2.58 70 022		2.63 60 300	2.65 100 300	2.53 17 202 2.64 90 022	2.54 60 031 2.63 20 -123	
		2.6	4		2.73 100 111	2.61 100 -121 2.66 45 120	2.66 100 -130 2.75 60 -101	2.69 100 111				
		2.8	1			2.84 70 -112				2.87 100 311	2.78 80 -104 2.81 80 120 2.92 60 -122	2.77 100 200

* only distances corresponding to I≥10 are reported

Table B: Comparison of the d-spacings measured by HRTEM on silver aggregates in aged Ag(4.1)/Al$_2$O$_3$ sample and on silver NPs in aged Ag(3)/Al$_2$O$_3$ sample with references of Al-based compounds

Silver NPs		Silver aggregates		γ-Al$_2$O$_3$ 10-0425 (blank) *			AlO(OH) 83-2384 (calculated)		
d (Å)	Measure number	d (Å)	Measure number	d (Å)	I	hkl	d (Å)	I	hkl
		1.4	3	1.4	100	440	1.43	4	002
				1.52	30	511			
		1.9	2						
2.0	1	2.0 2.1	11 6	1.98	100	400	1.98	3	131
		2.2	3						
2.3	12	2.3 2.35	7 3	2.28	50	222	2.34	25	031
		2.4	2	2.39	80	311			
		2.5 2.6	4 4						
		2.8	1	2.80	20	220			

* only distances corresponding to I≥10

Comments on HRTEM measurements

The most frequently measured distances at 2.0-2.1 and 2.3-2.4 Å fit very well with the lattice distances of the two most dense planes of Ag^0, (111) and (200), with d$_{111}$=2.35 Å and d$_{200}$=2.04 Å, respectively (**Table A SupInf5**). They also fit more or less with lattice distances of monoclinic Ag$_2$CO$_3$, but corresponding to peaks of low intensity.

The presence of Ag$_2$O as the main Ag compound can be discarded because its most dense plane is at 2.73 Å, so beyond the values measured and the other distances at 1.44, 1.67 and 2.36 Å correspond to too high index planes to be detectable (I <30).

The d-spacing at 1.4 Å measured in a few cases can fit with the (220) plan of Ag^0 but also with the (440) dense plane of γ-alumina (**Table B SupInf5**). The d-spacing at 1.9 Å found twice is close to inter-reticular distances of the other dense plane (400) of γ-alumina at 1.98 Å. However, the assignment to alumina can be discarded because (i) Ag is by far the main element detected on the particles by X-EDS (**SupInf4**), and (ii) the fringes are no more visible beyond the perimeter of the particles, indicating that they belong to the Ag particles and not to the support. Hence, the distances at 1.9 and 2.2 Å measured in a few cases can probably be considered as the very extreme values of the error bar of the distances at 2.0 and 2.3 Å of Ag^0. Indeed, the orientation of the particles with respect to the beam is not always exactly in the Bragg conditions, so measurements are not very accurate.

The lattice spacings at 2.5 and 2.6 Å measured several times could fit with the inter-reticular distances of several dense planes of Ag$_2$S at 2.58 and 2.60 Å or of Ag$_2$SO$_4$ at 2.53 and 2.64 Å. Note that the measured lattice fringes do not fit with those of AgCl, and that almost all of the lattice distances measured fit with those of Ag$_2$SO$_3$. However, the very low amount of sulfur detected by X-EDS (**SupInf4**) in areas containing Ag aggregates and in areas with no visible Ag particles, allows us to discard the presence of these three Ag species in the aged samples.

SupInf6: EXAFS

Table: Crystallographic parameters of Ag compounds and calculated Ag-O and Ag-Ag distances used for FEFF calculations.

Substance	Ag-O (Å)	Ag-Ag (Å)	a (Å)	b (Å)	c (Å)	$\alpha = \beta = \gamma$	Space group
Ag_2O[a]	2.048	3.345	4.718	4.718	4.718	90 °	P n -3 m :2
$AgNO_3$[b]	2.485 2.570	3.238	6.995	7.328	10.118	90 °	P b c a
$AgAlO_2$[c]	2.354	3.214	5.4306	6.9802	5.3751	90 °	P n a 21
Ag	-	2.889	4.0862	4.0862	4.0862	90 °	F m -3 m

a. P. Norby; R. Dinnebier; A. N. Fitch. *Inorganic Chemistry*. **2002**, 41, 3628-3637.

b. Trotter, J.; Gibbons, C.S. *Journal of the Chemical Society A: Inorganic, Physical, Theoretical*. **1971**, 2058-2062.

c. Li, J.; Sleight, A.W. *Journal of Solid State Chemistry*. **2004**, 177, 889-894

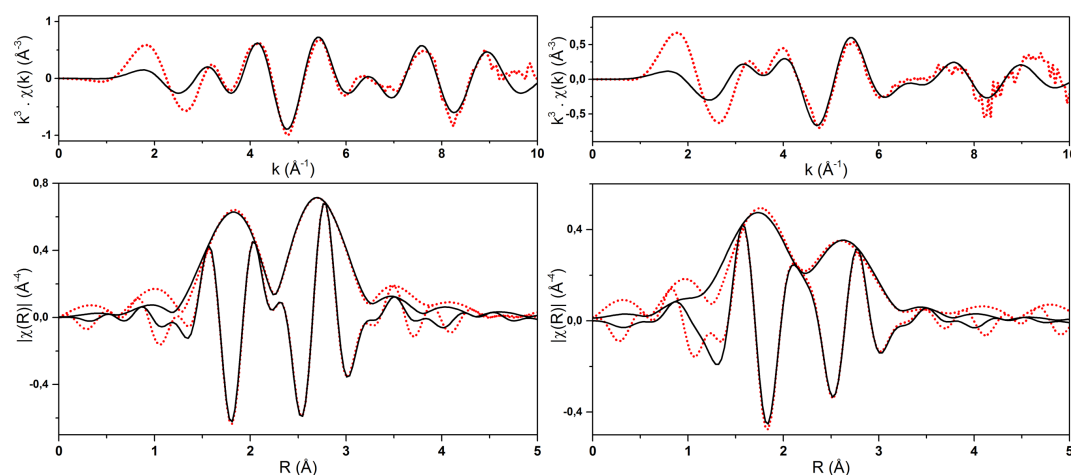d. Wyckoff, R. W. G. *Crystal Structures*. **1963**, 1, 7-83

Figure A: Ag K-edge $\chi(R)$ k^3-weighted fittings in k^3-space (top) and real and imaginary parts of R^3-space (bottom) of Ag/Al_2O_3 aged (left) and calcined (right) samples. (Δk = 3.3 - 9.0 Å^{-1})
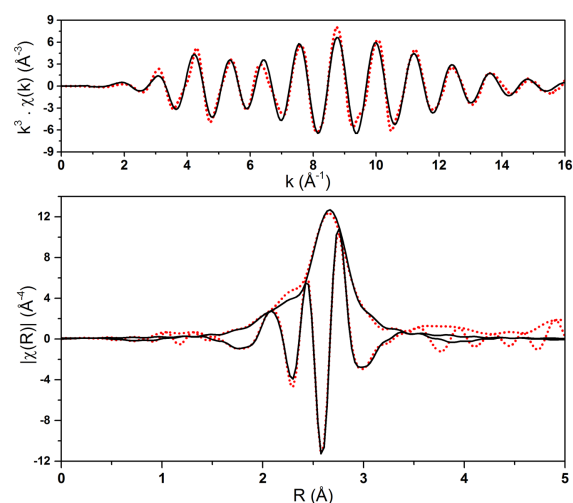

Figure B: Ag K-edge $\chi(R)$ k^3-weighted fittings of Ag foil. Parameters: Δk = 3.1 - 15.4 Å^{-1}, ΔR = 1.5-3.4 Å, N = 12. Results: S_0 = 0.82 ± 0.3, R = 2.883 ± 0.002 Å, σ^2 = 9,9 ± 0.2 Å^2, ΔE = 3.0 ± 0.2 eV and R factor = 0.0039.